EUROPEAN ORGANIZATION FOR NUCLEAR RESEARCH

CERN–EP-2000-043

08 February 2000

Measurement of the B_s^0 Lifetime and Study of B_s^0-$\overline{B_s^0}$ Oscillations using $D_s\ell$ Events

DELPHI Collaboration

Abstract

Lifetime and oscillations of B_s^0 mesons have been studied in events with a large transverse momentum lepton and a D_s of opposite electric charge in the same hemisphere, selected from about 3.6 million hadronic Z^0 decays accumulated by DELPHI between 1992 and 1995.
The B_s^0 lifetime and the fractional width difference between the two physical B_s^0 states have been found to be:

$$\tau_{B_s^0} = (1.42^{+0.14}_{-0.13}(stat.) \pm 0.03(syst.))\ ps$$

$$\Delta,_{B_s^0}/,_{B_s^0} < 0.46 \text{ at the } 95\% \text{ C.L.}$$

In the latter result it has been assumed that $\tau_{B_s^0} = \tau_{B_d^0}$.
Using the same sample, a limit on the mass difference between the physical B_s^0 states has been set:

$$\Delta m_{B_s^0} > 7.4 \text{ ps}^{-1} \text{ at the } 95\% \text{ C.L.}$$

with a corresponding sensitivity equal to 8.1 ps^{-1}.

(Submitted to E. Phys. J. C)

P.Abreu[21], W.Adam[50], T.Adye[36], P.Adzic[11], Z.Albrecht[17], T.Alderweireld[2], G.D.Alekseev[16], R.Alemany[49], T.Allmendinger[17], P.P.Allport[22], S.Almehed[24], U.Amaldi[??], N.Amapane[45], S.Amato[47], E.G.Anassontzis[3], P.Andersson[44], A.Andreazza[9], S.Andringa[21], P.Antilogus[25], W-D.Apel[17], Y.Arnoud[9], B.Åsman[44], J-E.Augustin[25], A.Augustinus[9], P.Baillon[9], P.Bambade[19], F.Barao[21], G.Barbiellini[46], R.Barbier[25], D.Y.Bardin[16], G.Barker[17], A.Baroncelli[38], M.Battaglia[15], M.Baubillier[23], K-H.Becks[52], M.Begalli[6], A.Behrmann[52], P.Beilliere[8], Yu.Belokopytov[9,53], K.Belous[42], N.C.Benekos[31], A.C.Benvenuti[5], C.Berat[14], M.Berggren[25], D.Bertini[25], D.Bertrand[2], M.Besancon[39], M.Bigi[45], M.S.Bilenky[16], M-A.Bizouard[19], D.Bloch[10], H.M.Blom[30], M.Bonesini[27], W.Bonivento[27], M.Boonekamp[39], P.S.L.Booth[22], A.W.Borgland[4], G.Borisov[19], C.Bosio[41], O.Botner[48], E.Boudinov[30], B.Bouquet[19], C.Bourdarios[19], T.J.V.Bowcock[22], I.Boyko[16], I.Bozovic[11], M.Bozzo[13], M.Bracko[43], P.Branchini[38], T.Brenke[52], R.A.Brenner[48], P.Bruckman[9], J-M.Brunet[8], L.Bugge[32], T.Buran[32], T.Burgsmueller[52], B.Buschbeck[50], P.Buschmann[52], S.Cabrera[49], M.Caccia[27], M.Calvi[27], T.Camporesi[9], V.Canale[37], F.Carena[9], L.Carroll[22], C.Caso[13], M.V.Castillo Gimenez[49], A.Cattai[9], F.R.Cavallo[5], V.Chabaud[9], M.Chapkin[42], Ph.Charpentier[9], L.Chaussard[25], P.Checchia[35], G.A.Chelkov[16], R.Chierici[45], P.Chliapnikov[42], P.Chochula[7], V.Chorowicz[25], J.Chudoba[29], K.Cieslik[18], P.Collins[9], R.Contri[13], E.Cortina[49], G.Cosme[19], F.Cossutti[9], H.B.Crawley[1], D.Crennell[36], S.Crepe[14], G.Crosetti[13], J.Cuevas Maestro[33], S.Czellar[15], M.Davenport[9], W.Da Silva[23], A.Deghorain[2], G.Della Ricca[46], P.Delpierre[26], N.Demaria[9], A.De Angelis[9], W.De Boer[17], C.De Clercq[2], B.De Lotto[46], A.De Min[35], L.De Paula[47], H.Dijkstra[9], L.Di Ciaccio[37,9], J.Dolbeau[8], K.Doroba[51], M.Dracos[10], J.Drees[52], M.Dris[31], A.Duperrin[25], J-D.Durand[9], G.Eigen[4], T.Ekelof[48], G.Ekspong[44], M.Ellert[48], M.Elsing[9], J-P.Engel[10], M.Espirito Santo[21], G.Fanourakis[11], D.Fassouliotis[11], J.Fayot[23], M.Feindt[17], A.Fenyuk[42], P.Ferrari[27], A.Ferrer[49], E.Ferrer-Ribas[19], F.Ferro[13], S.Fichet[23], A.Firestone[1], U.Flagmeyer[52], H.Foeth[9], E.Fokitis[31], F.Fontanelli[13], B.Franek[36], A.G.Frodesen[4], R.Fruhwirth[50], F.Fulda-Quenzer[19], J.Fuster[49], A.Galloni[22], D.Gamba[45], S.Gamblin[19], M.Gandelman[47], C.Garcia[49], C.Gaspar[9], M.Gaspar[47], U.Gasparini[35], Ph.Gavillet[9], E.N.Gazis[31], D.Gele[10], N.Ghodbane[25], I.Gil[49], F.Glege[52], R.Gokieli[9,51], B.Golob[43], G.Gomez-Ceballos[40], P.Goncalves[21], I.Gonzalez Caballero[40], G.Gopal[36], L.Gorn[1,54], Yu.Gouz[42], V.Gracco[13], J.Grahl[1], E.Graziani[38], H-J.Grimm[17], P.Gris[39], G.Grosdidier[19], K.Grzelak[51], M.Gunther[48], J.Guy[36], F.Hahn[9], S.Hahn[52], S.Haider[9], A.Hallgren[48], K.Hamacher[52], J.Hansen[32], F.J.Harris[34], V.Hedberg[24], S.Heising[17], J.J.Hernandez[49], P.Herquet[2], H.Herr[9], T.L.Hessing[34], J.-M.Heuser[52], E.Higon[49], S-O.Holmgren[44], P.J.Holt[34], S.Hoorelbeke[2], M.Houlden[22], J.Hrubec[50], K.Huet[2], G.J.Hughes[22], K.Hultqvist[44], J.N.Jackson[22], R.Jacobsson[9], P.Jalocha[18], R.Janik[7], Ch.Jarlskog[24], G.Jarlskog[24], P.Jarry[39], B.Jean-Marie[19], E.K.Johansson[44], P.Jonsson[25], C.Joram[9], P.Juillot[10], F.Kapusta[23], K.Karafasoulis[11], S.Katsanevas[25], E.C.Katsoufis[31], R.Keranen[17], G.Kernel[43], B.P.Kersevan[43], B.A.Khomenko[16], N.N.Khovanski[16], A.Kiiskinen[15], B.King[22], A.Kinvig[22], N.J.Kjaer[30], O.Klapp[52], H.Klein[9], P.Kluit[30], P.Kokkinias[11], M.Koratzinos[9], V.Kostioukhine[42], C.Kourkoumelis[3], O.Kouznetsov[39], M.Krammer[50], E.Kriznic[43], J.Krstic[11], Z.Krumstein[16], P.Kubinec[7], J.Kurowska[51], K.Kurvinen[15], J.W.Lamsa[1], D.W.Lane[1], P.Langefeld[52], V.Lapin[42], J-P.Laugier[39], R.Lauhakangas[15], G.Leder[50], F.Ledroit[14], V.Lefebure[2], L.Leinonen[44], A.Leisos[11], R.Leitner[29], G.Lenzen[52], V.Lepeltier[19], T.Lesiak[18], M.Lethuillier[39], J.Libby[34], D.Liko[9], A.Lipniacka[44], I.Lippi[35], B.Loerstad[24], J.G.Loken[34], J.H.Lopes[47], J.M.Lopez[40], R.Lopez-Fernandez[14], D.Loukas[11], P.Lutz[39], L.Lyons[34], J.MacNaughton[50], J.R.Mahon[6], A.Maio[21], A.Malek[52], T.G.M.Malmgren[44], S.Maltezos[31], V.Malychev[16], F.Mandl[50], J.Marco[40], R.Marco[40], B.Marechal[47], M.Margoni[35], J-C.Marin[9], C.Mariotti[9], A.Markou[11], C.Martinez-Rivero[19], F.Martinez-Vidal[49], S.Marti i Garcia[9], J.Masik[12], N.Mastroyiannopoulos[11], F.Matorras[40], C.Matteuzzi[27], G.Matthiae[37], F.Mazzucato[35], M.Mazzucato[35], M.Mc Cubbin[22], R.Mc Kay[1], R.Mc Nulty[22], G.Mc Pherson[22], C.Meroni[27], W.T.Meyer[1], E.Migliore[9], L.Mirabito[25], W.A.Mitaroff[50], U.Mjoernmark[24], T.Moa[44], M.Moch[17], R.Moeller[28], K.Moenig[9], M.R.Monge[13], X.Moreau[23], P.Morettini[13], G.Morton[34], U.Mueller[52], K.Muenich[52], M.Mulders[30], C.Mulet-Marquis[14], R.Muresan[24], W.J.Murray[36], B.Muryn[14,18], G.Myatt[34], T.Myklebust[32], F.Naraghi[14], M.Nassiakou[11], F.L.Navarria[5], S.Navas[49], K.Nawrocki[51], P.Negri[27], S.Nemecek[12], N.Neufeld[9], R.Nicolaidou[39], B.S.Nielsen[28], P.Niezurawski[51], M.Nikolenko[10,16], V.Nomokonov[15], A.Nygren[24], V.Obraztsov[42], A.G.Olshevski[16], A.Onofre[21], R.Orava[15], G.Orazi[10], K.Osterberg[15], A.Ouraou[39], M.Paganoni[27], S.Paiano[5], R.Pain[23], R.Paiva[21], J.Palacios[34], H.Palka[18], Th.D.Papadopoulou[31,9], K.Papageorgiou[11], L.Pape[9], C.Parkes[9], F.Parodi[13], U.Parzefall[22], A.Passeri[38], O.Passon[52], T.Pavel[24], M.Pegoraro[35], L.Peralta[21], M.Pernicka[50], A.Perrotta[5], C.Petridou[46], A.Petrolini[13], H.T.Phillips[36], F.Pierre[39], M.Pimenta[21], E.Piotto[27], T.Podobnik[43], M.E.Pol[6], G.Polok[18], P.Poropat[46], V.Pozdniakov[16], P.Privitera[37], N.Pukhaeva[16], A.Pullia[27], D.Radojicic[34], S.Ragazzi[27], H.Rahmani[31], P.N.Ratoff[20], A.L.Read[32], P.Rebecchi[9], N.G.Redaelli[27], M.Regler[50], D.Reid[30], R.Reinhardt[52], P.B.Renton[34], L.K.Resvanis[3], F.Richard[19], J.Ridky[12], G.Rinaudo[45], O.Rohne[32], A.Romero[45], P.Ronchese[35], E.I.Rosenberg[1], P.Rosinsky[7], P.Roudeau[19], T.Rovelli[5], Ch.Royon[39], V.Ruhlmann-Kleider[39], A.Ruiz[40], H.Saarikko[15], Y.Sacquin[39], A.Sadovsky[16], G.Sajot[14], J.Salt[49], D.Sampsonidis[11], M.Sannino[13], H.Schneider[17], Ph.Schwemling[23], B.Schwering[52], U.Schwickerath[17], F.Scuri[46], P.Seager[20], Y.Sedykh[16], A.M.Segar[34], R.Sekulin[36], R.C.Shellard[6], M.Siebel[52], L.Simard[39], F.Simonetto[35], A.N.Sisakian[16], G.Smadja[25], O.Smirnova[24], G.R.Smith[36], O.Solovianov[42], A.Sopczak[17], R.Sosnowski[51], T.Spassov[21], E.Spiriti[38], P.Sponholz[52], S.Squarcia[13], C.Stanescu[38], S.Stanic[43], K.Stevenson[34], A.Stocchi[19], J.Strauss[50], R.Strub[10], B.Stugu[4], M.Szczekowski[51], M.Szeptycka[51], T.Tabarelli[27], A.Taffard[22], F.Tegenfeldt[48], F.Terranova[27], J.Thomas[34], J.Timmermans[30], N.Tinti[5], L.G.Tkatchev[16], M.Tobin[22], S.Todorova[10], A.Tomaradze[2], B.Tome[21], A.Tonazzo[9], L.Tortora[38], G.Transtromer[24], D.Treille[9],

G.Tristram[8], M.Trochimczuk[51], C.Troncon[27], A.Tsirou[9], M-L.Turluer[39], I.A.Tyapkin[16], S.Tzamarias[11], O.Ullaland[9], V.Uvarov[42], G.Valenti[5], E.Vallazza[46], G.W.Van Apeldoorn[30], P.Van Dam[30], W.K.Van Doninck[2], J.Van Eldik[30], A.Van Lysebetten[2], N.Van Remortel[2], I.Van Vulpen[30], N.Vassilopoulos[34], G.Vegni[27], L.Ventura[35], W.Venus[36,9], F.Verbeure[2], M.Verlato[35], L.S.Vertogradov[16], V.Verzi[37], D.Vilanova[39], L.Vitale[46], E.Vlasov[42], A.S.Vodopyanov[16], C.Vollmer[17], G.Voulgaris[3], V.Vrba[12], H.Wahlen[52], C.Walck[44], A.J.Washbrook[22], C.Weiser[17], D.Wicke[52], J.H.Wickens[2], G.R.Wilkinson[9], M.Winter[10], M.Witek[18], G.Wolf[9], J.Yi[1], O.Yushchenko[42], A.Zaitsev[42], A.Zalewska[18], P.Zalewski[51], D.Zavrtanik[43], E.Zevgolatakos[11], N.I.Zimin[16,24], A.Zintchenko[16], G.C.Zucchelli[44], G.Zumerle[35]

[1] Department of Physics and Astronomy, Iowa State University, Ames IA 50011-3160, USA
[2] Physics Department, Univ. Instelling Antwerpen, Universiteitsplein 1, BE-2610 Wilrijk, Belgium
and IIHE, ULB-VUB, Pleinlaan 2, BE-1050 Brussels, Belgium
and Faculté des Sciences, Univ. de l'Etat Mons, Av. Maistriau 19, BE-7000 Mons, Belgium
[3] Physics Laboratory, University of Athens, Solonos Str. 104, GR-10680 Athens, Greece
[4] Department of Physics, University of Bergen, Allégaten 55, NO-5007 Bergen, Norway
[5] Dipartimento di Fisica, Università di Bologna and INFN, Via Irnerio 46, IT-40126 Bologna, Italy
[6] Centro Brasileiro de Pesquisas Físicas, rua Xavier Sigaud 150, BR-22290 Rio de Janeiro, Brazil
and Depto. de Física, Pont. Univ. Católica, C.P. 38071 BR-22453 Rio de Janeiro, Brazil
and Inst. de Física, Univ. Estadual do Rio de Janeiro, rua São Francisco Xavier 524, Rio de Janeiro, Brazil
[7] Comenius University, Faculty of Mathematics and Physics, Mlynska Dolina, SK-84215 Bratislava, Slovakia
[8] Collège de France, Lab. de Physique Corpusculaire, IN2P3-CNRS, FR-75231 Paris Cedex 05, France
[9] CERN, CH-1211 Geneva 23, Switzerland
[10] Institut de Recherches Subatomiques, IN2P3 - CNRS/ULP - BP20, FR-67037 Strasbourg Cedex, France
[11] Institute of Nuclear Physics, N.C.S.R. Demokritos, P.O. Box 60228, GR-15310 Athens, Greece
[12] FZU, Inst. of Phys. of the C.A.S. High Energy Physics Division, Na Slovance 2, CZ-180 40, Praha 8, Czech Republic
[13] Dipartimento di Fisica, Università di Genova and INFN, Via Dodecaneso 33, IT-16146 Genova, Italy
[14] Institut des Sciences Nucléaires, IN2P3-CNRS, Université de Grenoble 1, FR-38026 Grenoble Cedex, France
[15] Helsinki Institute of Physics, HIP, P.O. Box 9, FI-00014 Helsinki, Finland
[16] Joint Institute for Nuclear Research, Dubna, Head Post Office, P.O. Box 79, RU-101 000 Moscow, Russian Federation
[17] Institut für Experimentelle Kernphysik, Universität Karlsruhe, Postfach 6980, DE-76128 Karlsruhe, Germany
[18] Institute of Nuclear Physics and University of Mining and Metalurgy, Ul. Kawiory 26a, PL-30055 Krakow, Poland
[19] Université de Paris-Sud, Lab. de l'Accélérateur Linéaire, IN2P3-CNRS, Bât. 200, FR-91405 Orsay Cedex, France
[20] School of Physics and Chemistry, University of Lancaster, Lancaster LA1 4YB, UK
[21] LIP, IST, FCUL - Av. Elias Garcia, 14-1^{o}, PT-1000 Lisboa Codex, Portugal
[22] Department of Physics, University of Liverpool, P.O. Box 147, Liverpool L69 3BX, UK
[23] LPNHE, IN2P3-CNRS, Univ. Paris VI et VII, Tour 33 (RdC), 4 place Jussieu, FR-75252 Paris Cedex 05, France
[24] Department of Physics, University of Lund, Sölvegatan 14, SE-223 63 Lund, Sweden
[25] Université Claude Bernard de Lyon, IPNL, IN2P3-CNRS, FR-69622 Villeurbanne Cedex, France
[26] Univ. d'Aix - Marseille II - CPP, IN2P3-CNRS, FR-13288 Marseille Cedex 09, France
[27] Dipartimento di Fisica, Università di Milano and INFN, Via Celoria 16, IT-20133 Milan, Italy
[28] Niels Bohr Institute, Blegdamsvej 17, DK-2100 Copenhagen Ø, Denmark
[29] NC, Nuclear Centre of MFF, Charles University, Areal MFF, V Holesovickach 2, CZ-180 00, Praha 8, Czech Republic
[30] NIKHEF, Postbus 41882, NL-1009 DB Amsterdam, The Netherlands
[31] National Technical University, Physics Department, Zografou Campus, GR-15773 Athens, Greece
[32] Physics Department, University of Oslo, Blindern, NO-1000 Oslo 3, Norway
[33] Dpto. Fisica, Univ. Oviedo, Avda. Calvo Sotelo s/n, ES-33007 Oviedo, Spain
[34] Department of Physics, University of Oxford, Keble Road, Oxford OX1 3RH, UK
[35] Dipartimento di Fisica, Università di Padova and INFN, Via Marzolo 8, IT-35131 Padua, Italy
[36] Rutherford Appleton Laboratory, Chilton, Didcot OX11 OQX, UK
[37] Dipartimento di Fisica, Università di Roma II and INFN, Tor Vergata, IT-00173 Rome, Italy
[38] Dipartimento di Fisica, Università di Roma III and INFN, Via della Vasca Navale 84, IT-00146 Rome, Italy
[39] DAPNIA/Service de Physique des Particules, CEA-Saclay, FR-91191 Gif-sur-Yvette Cedex, France
[40] Instituto de Fisica de Cantabria (CSIC-UC), Avda. los Castros s/n, ES-39006 Santander, Spain
[41] Dipartimento di Fisica, Università degli Studi di Roma La Sapienza, Piazzale Aldo Moro 2, IT-00185 Rome, Italy
[42] Inst. for High Energy Physics, Serpukov P.O. Box 35, Protvino, (Moscow Region), Russian Federation
[43] J. Stefan Institute, Jamova 39, SI-1000 Ljubljana, Slovenia and Laboratory for Astroparticle Physics,
Nova Gorica Polytechnic, Kostanjeviska 16a, SI-5000 Nova Gorica, Slovenia,
and Department of Physics, University of Ljubljana, SI-1000 Ljubljana, Slovenia
[44] Fysikum, Stockholm University, Box 6730, SE-113 85 Stockholm, Sweden
[45] Dipartimento di Fisica Sperimentale, Università di Torino and INFN, Via P. Giuria 1, IT-10125 Turin, Italy
[46] Dipartimento di Fisica, Università di Trieste and INFN, Via A. Valerio 2, IT-34127 Trieste, Italy
and Istituto di Fisica, Università di Udine, IT-33100 Udine, Italy
[47] Univ. Federal do Rio de Janeiro, C.P. 68528 Cidade Univ., Ilha do Fundão BR-21945-970 Rio de Janeiro, Brazil
[48] Department of Radiation Sciences, University of Uppsala, P.O. Box 535, SE-751 21 Uppsala, Sweden
[49] IFIC, Valencia-CSIC, and D.F.A.M.N., U. de Valencia, Avda. Dr. Moliner 50, ES-46100 Burjassot (Valencia), Spain
[50] Institut für Hochenergiephysik, Österr. Akad. d. Wissensch., Nikolsdorfergasse 18, AT-1050 Vienna, Austria
[51] Inst. Nuclear Studies and University of Warsaw, Ul. Hoza 69, PL-00681 Warsaw, Poland
[52] Fachbereich Physik, University of Wuppertal, Postfach 100 127, DE-42097 Wuppertal, Germany
[53] On leave of absence from IHEP Serpukhov
[54] Now at University of Florida

1 Introduction

In this paper, the average lifetime of the B_s^0 meson has been measured and limits have been derived on the oscillation frequency of the B_s^0-$\overline{B_s^0}$ system, $\Delta m_{B_s^0}$, and on the decay width difference, $\Delta\Gamma_{B_s^0}$, between mass eigenstates of this system.
Starting with a B_s^0 meson produced at time t=0, the probability, $\mathcal{P}$, to observe a B_s^0 or a $\overline{B_s^0}$ decaying at the proper time t can be written, neglecting effects from CP violation:

$$\mathcal{P}[B_s^0 \to B_s^0(\overline{B_s^0})] \;=\; \frac{\Gamma_{B_s^0}}{2} e^{-\Gamma_{B_s^0} t}[\cosh(\frac{\Delta\Gamma_{B_s^0}}{2} t) \;\pm\; \cos(\Delta m_{B_s^0} t)] \qquad (1)$$

where $\Gamma_{B_s^0} = (\Gamma^H_{B_s^0} + \Gamma^L_{B_s^0})/2$, $\Delta\Gamma_{B_s^0} = \Gamma^L_{B_s^0} - \Gamma^H_{B_s^0}$ and $\Delta m_{B_s^0} = m^H_{B_s^0} - m^L_{B_s^0}$. L and H denote the light and heavy physical states, respectively; $\Delta\Gamma_{B_s^0}$ and $\Delta m_{B_s^0}$ are defined to be positive [1] and the plus (minus) signs refer to B_s^0 ($\overline{B_s^0}$) decays. The oscillation period gives a direct measurement of the mass difference between the two physical states. The Standard Model predicts that $\Delta\Gamma_{B_s^0} \ll \Delta m_{B_s^0}$, for which the previous expression simplifies to :

$$\mathcal{P}^{unmix.}_{B_s^0} \;=\; \mathcal{P}(B_s^0 \to B_s^0) \;=\; \Gamma_{B_s^0} e^{-\Gamma_{B_s^0} t} \cos^2(\frac{\Delta m_{B_s^0} t}{2}) \qquad (2)$$

and similarly:

$$\mathcal{P}^{mix.}_{B_s^0} = \mathcal{P}(B_s^0 \to \overline{B_s^0}) \;=\; \Gamma_{B_s^0} e^{-\Gamma_{B_s^0} t} \sin^2(\frac{\Delta m_{B_s^0} t}{2}) \qquad (3)$$

The oscillation frequency, proportional to $\Delta m_{B_s^0}$, can be obtained from the fit of the time distributions given in relations (2) and (3), whereas expression (1), without distinguishing between the B_s^0 and the $\overline{B_s^0}$, can be used to determine the average lifetime and the difference between the lifetimes of the heavy and light mass eigenstates.

B physics allows a precise determination of some of the parameters of the Cabibbo Kobayashi Maskawa (CKM) matrix. All the nine elements can be expressed in term of four parameters that are, in Wolfenstein parametrization [2], λ, A, ρ and η. The values of ρ and η are the most uncertain.
Several quantities which depend on ρ and η can be measured and, if the Standard Model is correct, they must define compatible values for the two parameters, inside measurement errors and theoretical uncertainties.
These quantities are ϵ_K, the parameter introduced to measure CP violation in the K system, $|V_{ub}|/|V_{cb}|$, the ratio between the modulus of the CKM matrix elements corresponding to $b \to u$ and $b \to c$ transitions and the mass difference $\Delta m_{B_d^0}$.

In the Standard Model, B_q^0-$\overline{B_q^0}$ ($q = d, s$) mixing is a direct consequence of second order weak interactions. Having kept only the dominant top quark contribution, $\Delta m_{B_q^0}$ can be expressed in terms of Standard Model parameters [3]:

$$\Delta m_{B_q^0} = \frac{G_F^2}{6\pi^2} |V_{tb}|^2 |V_{tq}|^2 m_t^2 m_{B_q} f^2_{B_q} B_{B_q} \eta_B F(\frac{m_t^2}{m_W^2}). \qquad (4)$$

In this expression G_F is the Fermi coupling constant; $F(x_t)$, with $x_t = \frac{m_t^2}{m_W^2}$, results from the evaluation of the second order weak "box" diagram responsible for the mixing and has a smooth dependence on x_t; η_B is a QCD correction factor obtained at next to leading order in perturbative QCD [4]. The dominant uncertainties in Equation (4) come from the evaluation of the B meson decay constant f_{B_q} and of the "bag" parameter B_{B_q}.

The mass differences $\Delta m_{\mathrm{B}^0_\mathrm{d}}$ and $\Delta m_{\mathrm{B}^0_\mathrm{s}}$ involve the CKM elements V_{td} and V_{ts}. Neglecting terms of order λ^4, these are given by:

$$|V_{td}| = A\lambda^3\sqrt{(1-\rho)^2+\eta^2} \quad ; \quad |V_{ts}| = A\lambda^2. \tag{5}$$

In the Wolfenstein parametrization, $|V_{ts}|$ is independent of ρ and η. A measurement of $\Delta m_{\mathrm{B}^0_\mathrm{s}}$ is thus a way to measure the value of the non perturbative QCD parameters. Direct information on V_{td} can be inferred by measuring $\Delta m_{\mathrm{B}^0_\mathrm{d}}$.
Several experiments have accurately measured $\Delta m_{\mathrm{B}^0_\mathrm{d}}$, nevertheless this precision cannot be fully exploited to extract information on ρ and η because of the large uncertainty which originates in the evaluation of the non-perturbative QCD parameters.
An efficient constraint is the ratio between the Standard Model expectations for $\Delta m_{\mathrm{B}^0_\mathrm{d}}$ and $\Delta m_{\mathrm{B}^0_\mathrm{s}}$, given by:

$$\frac{\Delta m_{\mathrm{B}^0_\mathrm{d}}}{\Delta m_{\mathrm{B}^0_\mathrm{s}}} = \frac{m_{\mathrm{B}^0_\mathrm{d}} f^2_{\mathrm{B}^0_\mathrm{d}} B_{\mathrm{B}^0_\mathrm{d}} \eta_{\mathrm{B}^0_\mathrm{d}}}{m_{\mathrm{B}^0_\mathrm{s}} f^2_{\mathrm{B}^0_\mathrm{s}} B_{\mathrm{B}^0_\mathrm{s}} \eta_{\mathrm{B}^0_\mathrm{s}}} \frac{|V_{td}|^2}{|V_{ts}|^2} \tag{6}$$

A measurement of the ratio $\Delta m_{\mathrm{B}^0_\mathrm{d}}/\Delta m_{\mathrm{B}^0_\mathrm{s}}$ gives the same type of constraint, in the $\rho-\eta$ plane, as a measurement of $\Delta m_{\mathrm{B}^0_\mathrm{d}}$, but because only ratio $f_{\mathrm{B}^0_\mathrm{d}}/f_{\mathrm{B}^0_\mathrm{s}}$ and $B_{\mathrm{B}^0_\mathrm{d}}/B_{\mathrm{B}^0_\mathrm{s}}$ are involved, some of the theoretical uncertainties cancel [5].
Using existing measurements which constrain ρ and η, except those on $\Delta m_{\mathrm{B}^0_\mathrm{s}}$, the distribution for the expected values of $\Delta m_{\mathrm{B}^0_\mathrm{s}}$ can be obtained. It has been shown, in the context of Standard Model and QCD assumptions, that $\Delta m_{\mathrm{B}^0_\mathrm{s}}$ has to lie, at 68% C.L., between 12 and 17.6 ps^{-1} and is expected to be smaller than $20ps^{-1}$ at 95% C.L. [6].

The B^0_s meson lifetime is expected to be equal to the B^0_d lifetime [1] within one percent. In the Standard Model, the ratio between the mass difference and decay width in the B^0-$\overline{\mathrm{B}^0}$ system is of the order $(m_b/m_t)^2$, although large QCD corrections are expected. Explicit calculations to leading order in QCD correction, in the HQE (Heavy Quark Expansion) formalism [1], predict:

$$\Delta,\ _{\mathrm{B}^0_\mathrm{s}}/,\ _{\mathrm{B}^0_\mathrm{s}} = 0.16^{+0.11}_{-0.09}$$

where the quoted error is dominated by the uncertainty related to hadronic matrix elements.
Recent calculations [7] at next-to-leading order predict a lower value:

$$\Delta,\ _{\mathrm{B}^0_\mathrm{s}}/,\ _{\mathrm{B}^0_\mathrm{s}} = 0.054^{+0.016}_{-0.032}$$

An interesting approach consists in using the ratio between $\Delta,\ _{\mathrm{B}^0_\mathrm{s}}$ and $\Delta m_{\mathrm{B}^0_\mathrm{s}}$ [7]:

$$\frac{\Delta,\ _{\mathrm{B}^0_\mathrm{s}}}{\Delta m_{\mathrm{B}^0_\mathrm{s}}} = (2.63^{+0.67}_{-1.36})10^{-3} \tag{7}$$

to constrain the upper part of the $\Delta m_{\mathrm{B}^0_\mathrm{s}}$ spectrum with an upper limit on $\Delta,\ _{\mathrm{B}^0_\mathrm{s}}/,\ _{\mathrm{B}^0_\mathrm{s}}$.
If, in future, the theoretical uncertainty can be reduced, this method can give an alternative approach in determining $\Delta m_{\mathrm{B}^0_\mathrm{s}}$ via $\Delta,\ _{\mathrm{B}^0_\mathrm{s}}$ and, in conjunction with the determination of $\Delta m_{\mathrm{B}^0_\mathrm{d}}$, can provide an extra constraint on the ρ and η parameters.

The results presented in the following have been obtained from data accumulated by DELPHI experiment at LEP between 1992 and 1995, corresponding to about 3.6 million hadronic Z^0 decays. The main features of these analyses are:

- a precise measurement of the B decay proper time;
- a determination of the charge of the b quark at the B-meson decay time (decay tag);
- a determination of the sign of the b quark at production time (production tag).

The first item is common to the three studies on $\Delta m_{\mathrm{B_s^0}}$, $\tau_{\mathrm{B_s^0}}$ and $\Delta,_{\mathrm{B_s^0}}$ while the others are specific to the oscillation analyses. For these last, the principle of the measurement is as follows. Each of the charged and neutral particles measured in an event is assigned to one of the two hemispheres defined by the plane transverse to the sphericity axis. A "production tag" is used to estimate the $\mathrm{b}/\overline{\mathrm{b}}$ sign of the initial quark at the production point. The decay time of the B hadron is evaluated and a "decay tag" is defined, correlated with the $\mathrm{b}/\overline{\mathrm{b}}$ content of the decaying hadron. The analysis is performed using events containing a lepton emitted at large transverse momentum, p_T, relative to its jet axis accompanied by an exclusively (or partially) reconstructed $\mathrm{D_s}$ in the same hemisphere and of opposite electric charge. The lepton charge defines the "decay tag". Different variables defined in the same and in the opposite hemisphere, are used to determine the "production tag".
Similar analyses have been performed by the ALEPH, CDF and OPAL Collaborations [8–10].

Section 2 describes the main features of the DELPHI detector, the event selection and the event simulation. Section 3 describes the selection of the $\mathrm{D_s}\ell$ sample. Section 4 presents the $\mathrm{B_s^0}$ lifetime measurement. Section 5 presents the result on the lifetime difference. Section 6 is devoted to the study of $\mathrm{B_s^0}$-$\overline{\mathrm{B_s^0}}$ oscillations with the $\mathrm{D_s}\ell$ sample: the first part describes the "production tag" algorithm while the second part presents the fitting procedure and the result on $\Delta m_{\mathrm{B_s^0}}$.

2 The DELPHI detector

The events used in this analysis have been recorded with the DELPHI detector at LEP operating at energies close to the $\mathrm{Z^0}$ peak. The DELPHI detector and its performance have been described in detail elsewhere [11]. In this section are summarized the most relevant characteristics for this analysis.

2.1 Global event reconstruction

2.1.1 Charged particles reconstruction

The detector elements used for tracking are the Vertex Detector (VD), the Inner Detector (ID), the Time Projection Chamber (TPC) and the Outer Detector (OD).

The VD provided the high precision needed near the primary vertex. For the data taken from 1991 to 1993, the VD consisted of three cylindrical layers of silicon detectors (radii 6.3, 9.0 and 10.9 cm) measuring points in the plane transverse to the beam direction ($r\phi$ coordinate) in the polar angle range $43^\circ < \theta < 137^\circ$. In 1994, two layers have been equipped with detector modules with double sided readout, providing a single hit precision of 7.6 μm in the $r\phi$ coordinate, similar to that obtained previously, and 9 μm in the coordinate parallel to the beam (z) [12]. For high momentum particles with associated hits in the VD, the extrapolation precision close to the interaction region is 20 μm in the $r\phi$ plane and 34 μm in the rz plane.

Charged particle tracks have been reconstructed with 95% efficiency and with a momentum resolution $\sigma_p/p < 2.0 \times 10^{-3} p$ (p in GeV/c) in the polar angle region $25^\circ < \theta < 155^\circ$.

2.1.2 Energy reconstruction

The total energy in the event is determined by using all information available from the tracking detectors and the calorimeters. For charged particles, the momentum measured in the tracking detector is used. Photons are detected and their energy measured in the electromagnetic calorimeters, whereas the hadron calorimeter detects long lived neutral hadrons such as neutrons and K_L^0's.

The electromagnetic calorimetry system of DELPHI is composed of a barrel calorimeter, the HPC, covering the polar angle region $46° < \theta < 134°$, and a forward calorimeter, the FEMC, for polar angles $8° < \theta < 35°$ and $145° < \theta < 172°$. The relative precision on the measured energy E has been parametrized as $\sigma_E/E = 0.32/\sqrt{E} \oplus 0.043$ (E in GeV) in the barrel, and $\sigma_E/E = 0.12/\sqrt{E} \oplus 0.03$ (E in GeV) in the forward region.

The hadronic calorimeter, HCAL, has been installed in the return yoke of the DELPHI solenoid. In the barrel region, the energy has been reconstructed with a precision of $\sigma_E/E = 1.12/\sqrt{E} \oplus 0.21$ (E in GeV).

2.1.3 Hadronic Z^0 selection

Hadronic events from Z^0 decays have been selected by requiring a charged multiplicity greater than four and a total energy of charged particles greater than $0.12\sqrt{s}$, where $\sqrt{s}$ is the centre-of-mass energy and all particles have been assumed to be pions; charged particles have been required to have a momentum greater than 0.4 GeV/c and a polar angle between 20° and 160°. The overall trigger and selection efficiency is (95.0±0.1)% [13]. A total of about 3.6 million hadronic events has been obtained from the 1992-1995 data.

2.2 Particle identification

2.2.1 Lepton identification

Lepton identification in the DELPHI detector is based on the barrel electromagnetic calorimeter and the muon chambers. Only particles with momentum larger than 2 GeV/c have been considered as possible lepton candidates.

Muon chambers consisted, in the barrel region, of three layers covering the polar regions $53° < \theta < 88.5°$ and $91.5° < \theta < 127°$. The first layer contained three planes of chambers and was inside the return yoke of the magnet after 90 cm of iron, while the other two, with two chamber planes each, were mounted outside the yoke behind a further 20 cm of iron. In the end-caps there were two layers of muon chambers mounted one outside and one inside the return yoke of the magnet. Each consisted of two planes of active chambers covering the polar angle regions $20° < \theta < 42°$ and $138° < \theta < 160°$ where the charged particle tracking was efficient.

The probability of a particle being a muon has been calculated from a global χ^2 of the match between the track extrapolation to the muon chambers and the hits observed there. Four identification flags are given as output of the muon identification in decreasing order of efficiency: very loose, loose, standard and tight. In this analysis the loose selection has been applied corresponding to an efficiency of $(94.8 \pm 0.1)\%$ with a hadron misidentification probability of $(1.5 \pm 0.1)\%$.

Electron identification has been performed using two independent and complementary measurements, the dE/dx measurement of the TPC (described in Section 2.2.2) and the energy deposition in the HPC. Probabilities from calorimetric measurements and tracking are combined to produce an overall probability for the electron hypothesis. Three levels

of identification are given: loose, standard and tight.
The loose selection has been applied for this analysis corresponding to an efficiency of 80 % with an hadron misidentifation probability of $\simeq$ 1.6 %.

2.2.2 Hadron identification

Hadron identification relied on the RICH detector and on the specific ionization measurement performed by the TPC.

The RICH detector [14] used two radiators. A gas radiator separated kaons from pions between 3 and 9 GeV/c, where kaons gave no Cherenkov light whereas pions did, and between 9 and 16 GeV/c, using the measured Cherenkov angle. It also provided kaon/proton separation from 8 to 20 GeV/c. A liquid radiator, which has been fully operational for 1994 and 1995 data, provided $p/K/\pi$ separation in the momentum range 1.5–7 GeV/c.

The specific energy loss per unit length (dE/dx) is measured in the TPC by using up to 192 sense wires. At least 30 contributing measurements have been required to compute the truncated mean. In the momentum range $3 < p < 25$ GeV/c, this is fulfilled for 55% of the tracks, and the dE/dx measurement has a precision of $\pm$7%.

The combination of the two measurements, dE/dx and RICH angles, provides three levels of pion, kaon and proton tag (loose, standard, tight) corresponding to different purities. A tag for "Heavy Particle" is also given in order to separate pions from heavier hadrons with high efficiency.
The Standard "Heavy Particle" flag has an efficiency of about 70 % with a pion misidentification probability of 10 % for charged particle with momentum greater than 0.7 GeV/c.

2.2.3 Λ^0 and K^0 reconstruction

The $\Lambda^0 \to p\pi^-$ and $K^0 \to \pi^+\pi^-$ decays have been reconstructed if the distance in the $r\phi$ plane between the V^0 decay point and the primary vertex is less than 90 cm. This condition meant that the decay products have track segments at least 20 cm long in the TPC. The reconstruction of the V^0 vertex and selection cuts are described in detail in reference [11].
Only K^0 candidates passing the "tight" selection criteria have been retained for this analysis.

2.2.4 π^0 reconstruction

The $\pi^0 \to \gamma\gamma$ decays are reconstructed by fitting all $\gamma\gamma$ pairs whose invariant mass is within 20 MeV of the nominal π^0 mass, using the nominal π^0 mass as a constraint. The fit probability has to be larger than 1%.

2.3 Primary vertex reconstruction and event topology

The location of the e^+e^- interaction has been reconstructed on an event-by-event basis using the beam spot position as a constraint [11]. In 1994 and 1995 data, the position of the primary vertex transverse to the beam has been determined with a precision of about 40 μm in the horizontal direction, and about 10 μm in the vertical direction. For 1992 and 1993 data, the uncertainties are larger by about 50%.

Each selected event has been divided into two hemispheres separated by the plane transverse to the sphericity axis. A clustering analysis based on the JETSET algorithm

LUCLUS [15] with default parameters has been used to define the jets, using both charged and neutral particles. These jets have been used to measure the P_T of each particle in the event, defined as its momentum transverse to the axis of the rest of the jet it belonged to, after removing the particle itself.

The different detector configurations, both for hadron identification and vertex resolution, implies, in the rest of the analysis, a separate treatment of the data taken before and after 1994.

2.4 b-tagging

The b-tagging package developed by the DELPHI collaboration has been described in reference [16]. The impact parameters of the charged particle tracks, with respect to the primary vertex, have been used to build the probability that all tracks come from this vertex. Due to the long B-hadrons lifetime, the probability distribution is peaked at zero for events which contained beauty whereas it is flat for events containing light quarks. The b-tagging algorithm has been used in this analysis to select control samples with low b purity.

2.5 Event simulation

Simulated events have been generated using the JETSET 7.3 program [15] with parameters tuned as in [17] and using an updated description of B decays. B hadron semileptonic decays have been simulated using the ISGW model [18]. Generated events have been followed through the full simulation of the DELPHI detector (DELSIM) [11], and the resulting simulated raw data have been processed through the same reconstruction and analysis programs as the real data.

3 The $\mathrm{D_s^{\pm}}\ell^{\mp}$ sample selection

$\overline{\mathrm{B_s^0}}$ semileptonic decays[1] have been selected requiring the presence of a $\mathrm{D_s^+}$ meson correlated with a high p_T lepton of opposite electric charge in the same hemisphere:

$$\overline{\mathrm{B_s^0}} \to \mathrm{D_s^+}\ell^-\overline{\nu_\ell}X.$$

The $\mathrm{D_s}$ mesons have been reconstructed in six non-leptonic and two semileptonic decay channels:

$$\begin{array}{ll}
\mathrm{D_s^+} \to \phi\pi^+ & \phi \to \mathrm{K^+K^-}; \\
\mathrm{D_s^+} \to \overline{\mathrm{K}}^{\star 0}\mathrm{K^+} & \overline{\mathrm{K}}^{\star 0} \to \mathrm{K^-}\pi^+; \\
\mathrm{D_s^+} \to \mathrm{K_S^0K^+} & \mathrm{K_S^0} \to \pi^+\pi^-; \\
\mathrm{D_s^+} \to \phi\pi^+\pi^-\pi^+ & \phi \to \mathrm{K^+K^-}; \\
\mathrm{D_s^+} \to \phi\pi^+\pi^0 & \phi \to \mathrm{K^+K^-}; \\
\mathrm{D_s^+} \to \overline{\mathrm{K}}^{\star 0}\mathrm{K}^{\star +} & \overline{\mathrm{K}}^{\star 0} \to \mathrm{K^-}\pi^+, \quad \mathrm{K}^{\star +} \to \mathrm{K_S^0}\pi^+;
\end{array}$$

$$\begin{array}{ll}
\mathrm{D_s^+} \to \phi e^+\nu_e & \phi \to \mathrm{K^+K^-}; \\
\mathrm{D_s^+} \to \phi\mu^+\nu_\mu & \phi \to \mathrm{K^+K^-}.
\end{array}$$

[1] Charge conjugation is always implied.

In addition, partially reconstructed D_s^+ have been selected requiring the presence of a ϕ meson (reconstructed in the K^+K^- decay channel) accompanied by an hadron h^+ in the same hemisphere.

$$D_s^+ \to \phi h^+ X$$

In the following the first eight decay modes will be referred as the $D_s\ell$ sample and the last one as the $\phi\ell h$ sample.

3.1 Selection of the $\phi\pi^+$, $\overline{K}^{*0}K^+$, $K_S^0K^+$ and $\phi\ell^+\nu$ decay modes

Each D_s decay mode has been reconstructed by making all possible combinations of particles in the same hemisphere. In D_s^+ semileptonic decays, the ambiguity between the two leptons has been removed by assigning the lepton to the D_s^+ ($\overline{B_s^0}$) if the mass of the $\phi\ell$ system, $M(\phi\ell)$, is below (above) the nominal D_s^+ mass. If the two leptons both gave a $M(\phi\ell)$ above or below the D_s mass, the event was rejected.
The measured position of the D_s^+ decay vertex and momentum together with their measurement errors, have been used to form a new track (called pseudo-track) that contains the measured parameters of the D_s^+ particle.
A candidate $\overline{B_s^0}$ decay vertex has been obtained by intercepting the D_s^+ pseudo-track with the one of a lepton. To guarantee a precise determination of the position of this secondary vertex, at least one VD hit has been required to be associated to the lepton and to at least two tracks from the D_s^+ decay products. The χ^2 of the reconstructed D_s^+ and $\overline{B_s^0}$ vertices have been required to be smaller than 40 and 20 respectively.
In order to suppress fake leptons and B hadron cascade decays ($b \to c \to \ell^+$), additional selection criteria have been applied to the $D_s\ell$ pairs, which are summarized in Table 1.
For the channel $D_s^+ \to \phi\ell^+\nu$ requirements on the $\phi\ell\ell$ mass and momentum have been reduced as compared to the other channels to account for the additional escaping neutrino. Due to the smaller combinatorial background under the D_s signal, in the $D_s \to \phi\pi^+$ and $D_s \to \phi\ell^+\nu$ decay channels, the p_T cut has been lowered to 1 GeV/c.

	$\phi\pi^+$	$\phi\ell^+$	Others
$p_T(\ell)(GeV/c)$	> 1	> 1	> 1.2
$M(D_s\ell)(GeV/c^2)$	$\in [3, 5.5]$	$\in [2.5, 5.5]$	$\in [3, 5.5]$
$P(D_s\ell)(GeV/c)$	> 14	> 12	> 14

Table 1: *Selection criteria applied to the lepton and* D_s *candidates.*

A tighter selection was then applied, separately for each decay mode, using a discriminant variable built with the variables listed in Table 2.
These variables are:

- the momenta, P, and masses, M, of the decay products;
- the cosine of the helicity angle, ψ, for the $\phi\pi^+$ and $\overline{K}^{*0}K^+$ decay modes;
- H_{ID}, defining whether the hadron identification from Section 2.2.2 favours the π, K or proton hypothesis;
- L_{ID}, defining whether the lepton identification from Section 2.2.1 identifies a particle from the D_s^+ semileptonic decay as an electron or a muon (used only for leptons coming from the D_s^+ semileptonic decays).

For each quantity the probability densities for the signal (S) ($D_s\ell$ from B_s^0 semileptonic decays) and for the combinatorial background (B) (fake $D_s\ell$ candidates in $q\overline{q}$ events) have been parametrized using the simulation; the discriminant variable X_{D_s} is then defined as

$$R = \prod_i R_i = \prod_i \frac{S_i(x_i)}{B_i(x_i)} \qquad X_{D_s} = \frac{R}{R+1}$$

where i runs over the number of variables (which actual values are x_i). The combinatorial background is concentrated close to $X_{D_s} = 0$ while the D_s signal accumulates close to $X_{D_s} = 1$. The definition of X_{D_s} provides an optimal separation between the signal and the combinatorial background if the individual discriminant variables x_i are independent; in case of correlations the separation power decreases but no bias is introduced.

$\phi\pi$	$\overline{K^{0*}}K$	K_S^0K	$\phi\ell^+$
$P(D_s)$	$P(D_s)$	$P(D_s)$	$P(\phi)$
$P(\phi)/P(D_s)$	$P(K^{*0})/P(D_s)$	$P(K_S^0)/P(D_s)$	
H_{ID} K_1	H_{ID} K_1	H_{ID} K	H_{ID} K_1
H_{ID} K_2	H_{ID} K_2		H_{ID} K_2
H_{ID} π	H_{ID} π		L_{ID} $\ell(D_s)$
$cos(\psi)$	$cos(\psi)$		
$M(\phi)$	$M(K^{*0})$		

Table 2: *List of the quantities which are used, in the different decay channels, to construct a discriminant variable between* B_s^0 *semileptonic decays and background events.*

The distributions of this variable obtained in data and in the simulation are shown in Figure 1 for the $\phi\pi^+$ decay channel.

The optimal value of the cut on the discriminant variable has been studied on simulated events, separately for each channel and for each detector configuration, in order to keep high efficiency (Table 3). A very loose cut has been applied on the $\phi\pi^+$ channel because of its small combinatorial background.

The individual event purity has been evaluated, in the following, from the distribution of the discriminant variable for signal and combinatorial background.

	$\phi\pi^+$	$\overline{K^{0*}}K$	K_S^0K	$\phi\ell^+$
92-93	> 0.05	> 0.75	> 0.80	> 0.75
94-95	> 0.03	> 0.85	> 0.90	> 0.90

Table 3: *Values of the cuts applied on the discriminant variable* X_{D_s} *to select* B_s^0 *semileptonic decay candidates.*

In addition, for the two channels ($\overline{K^{*0}}K$ and K_S^0K), which receive contributions from kinematic reflections of non strange B decays, the bachelor kaon has been required to be incompatible with the pion hypothesis.

Further background suppression has been obtained by placing a requirement on the D_s

flight distance $L(\mathrm{D_s})$. The small effect induced on the decay time acceptance has been taken into account in the following. This requirement has been applied, depending on the resolution on the decay distance observed in the different $\mathrm{D_s}$ decay channels and on the level of the combinatorial background: $L(\mathrm{D_s}) > 0$ for $\phi\pi$ and $\overline{\mathrm{K}^{*0}}\mathrm{K}^+$, $L(\mathrm{D_s})/\sigma(L(\mathrm{D_s})) > -3$ for $\mathrm{K^0_S K}^+$ and $L(\mathrm{D_s})/\sigma(L(\mathrm{D_s})) > -1$ for $\phi\ell^+$.
Finally, for the semileptonic decay modes (with two neutrinos in the final state) an algorithm has been developed to estimate the missing energy, E_{miss}, defined as:

$$E_{miss} = E_{tot} - E_{vis}$$

where the visible energy (E_{vis}) is the sum of the energies of charged particles and photons in the same hemisphere as the $\mathrm{D_s}\ell$ candidate. Using four-momentum conservation, the total energy (E_{tot}) in that hemisphere is:

$$E_{tot} = E_{beam} + \frac{M^2_{same} - M^2_{opp}}{4E_{beam}}$$

where M_{same} and M_{opp} are the hemisphere invariant masses of the same and opposite hemispheres respectively. A positive missing energy E_{miss} has been required.

3.2 Selection of the $\phi\pi^+\pi^+\pi^-$, $\phi\pi^+\pi^0$ and $\overline{\mathrm{K}}^{*0}\mathrm{K}^{*+}$ decay modes

These three decay modes have been searched for in the 94 and 95 data only.
$\mathrm{D_s}\ell$ pairs have been selected by requiring $M(\mathrm{D_s}\ell) > 3.0\ GeV/c^2$, $p_T(\ell) > 1.2\ GeV/c$ and χ^2 ($\mathrm{D_s}\ell$ vertex)< 20 (except for the $\phi\pi^+\pi^+\pi^-$ decay mode in which no χ^2 cut has been applied).
In each event only one candidate is kept. The procedure is the following: if more than one candidate passed all the selection criteria only the one with the highest lepton transverse momentum and, if the same lepton candidate is attached to several $\mathrm{D_s^+}$ candidates the highest $\mathrm{D_s^+}$ momentum, is kept.
It has been verified that this requirement keeps the signal with high efficiency and removes some of the combinatorial background.

3.2.1 $\mathrm{D_s^+} \to \overline{\mathrm{K}}^{*0}\mathrm{K}^{*+}$

$\mathrm{D_s^+}$ candidates have been selected by reconstructing $\overline{\mathrm{K}}^{*0} \to \mathrm{K}^-\pi^+$ and $\mathrm{K}^{*+} \to \mathrm{K^0_s}\pi^+$ decays. $\mathrm{K^0_s}$ candidates have been reconstructed in the mode $\mathrm{K^0_s} \to \pi^+\pi^-$ by combining all pairs of oppositely charged particles and applying the "tight" selection criteria described in [11]. The $\mathrm{K^0_s}$ has been then combined with two charged particles of the same sign, and a third with opposite charge. If more than one $\mathrm{D_s^+}$ candidate could be reconstructed by the same four particles (by swapping the two pion candidates for example) the $\mathrm{D_s^+}$ candidate minimizing the squared mass difference $(M(\mathrm{K}^-\pi^+) - M(\overline{\mathrm{K}}^{*0}))^2 + (M(\mathrm{K^0_s}\pi^+) - M(\mathrm{K}^{*+}))^2$ has been chosen, where $M(\overline{\mathrm{K}}^{*0})$ and $M(\mathrm{K}^{*+})$ are the nominal K^* masses [19]. The three charged particle tracks have been fitted to a common vertex and the χ^2 of this vertex has been required to be smaller than 30. To improve the resolution on the vertex position, all three tracks have been required to have at least one VD hit.
$\mathrm{K}^-\pi^+$ and $\mathrm{K^0_S}\pi^+$ mass combinations have been selected if their effective masses are within ± 75 and $\pm 95\ MeV/c^2$ of the nominal neutral and charged $\overline{\mathrm{K}^*}$ mass respectively.
The charged pion and kaon from $\overline{\mathrm{K}^*}$ decays must have a momentum larger than 1 and 1.5 GeV/c respectively. The charged and neutral $\overline{\mathrm{K}^*}$ mesons must have a momentum larger than 4 and 3.5 GeV/c respectively and $\mathrm{D_s^+}$ mesons have a momentum larger than 11 GeV/c.

3.2.2 $D_s^+ \to \phi\pi\pi\pi$

The ϕ is reconstructed in the decay channel $\phi \to K^+K^-$ by taking all possible pairs of oppositely charged particle tracks that have an invariant mass within 13 MeV/c^2 of the nominal ϕ meson mass [19]. Neither kaon candidate should be tagged by the combined RICH and dE/dX measurements as pions ("tight" selection). Three tracks, each compatible with the pion hypothesis as given by the combined RICH and dE/dX measurements, have been then added to the ϕ candidate to make a D_s^+. The five tracks have been required to be compatible with a single vertex, but no requirement has been applied on the χ^2 of the vertex fit. Three of the five tracks have been required to have at least one VD hit and two of the three pion candidates have been required to have a momentum above 1.2 GeV/c.

In addition, kaons from the ϕ decays must have a momentum larger than 1.8 GeV/c. Individual pion momenta must be larger than 700 MeV/c and the D_s candidate momentum must be larger than 9 GeV/c.

3.2.3 $D_s^+ \to \phi\pi\pi^0$

The ϕ is reconstructed using the same selection criteria as for the previous channel. A third track, which has been required not to be tagged as a kaon by the combined RICH and dE/dx, and a reconstructed π^0 (Section. 2.2.4) have been added to the ϕ candidate. The three charged tracks have been fitted to a common vertex. To improve the resolution on the vertex position, each of the three tracks has been required to be associated to at least one VD hit each.
In addition, kaons from the ϕ decay must have a momentum larger than 2.5 GeV/c. The momentum of the charged pion and of the D_s must be larger than 1 and 10 GeV/c respectively.

3.3 Summary for the $D_s\ell$ selected events

3.3.1 Non leptonic D_s modes

In the D_s^+ mass region, an excess of "right-sign" ($D_s^\pm \ell^\mp$) over "wrong-sign" ($D_s^\pm \ell^\pm$) combinations is observed in each channel (Figure 2). The estimated number of signal events and the yields for the combinatorial background in all the studied modes are summarized in Table 4. The mass distribution for non-leptonic decays has been fitted with two Gaussian distributions of equal widths to account for the D_s^+ and D^+ signals and a polynomial function for the combinatorial background. The D^+ mass has been fixed at the nominal value of 1.869 GeV/c^2 [19]. The overall mass distribution for non-leptonic decays is shown in (Figure 3a). The fit yields a signal of (206 ± 21) D_s decays in "right-sign" combinations, centred at a mass of (1.9680 ± 0.0016) GeV/c^2 with a width of (14 ± 1) MeV/c^2.

3.3.2 Semileptonic D_s modes

Selected events show an excess of "right-sign" with respect to "wrong-sign" combinations (Figure 3b). The K^+K^- invariant mass distribution for "right sign" events has been fitted with a Breit–Wigner distribution to account for the signal and a polynomial function to describe the combinatorial background. The fit gives (80 ± 16) events (see Table 4) centred at a mass of (1.020 ± 0.001) GeV/c^2 with a total width (,) of (5 ± 1) MeV/c^2.

D_s decay modes	Estimated signal	Combinatorial background / Total
$D_s \to \phi\pi^+$	83 ± 11	0.38 ± 0.06
$D_s \to \overline{K}^{*0}K^+$	60 ± 11	0.45 ± 0.06
$D_s \to K^0_S K^+$	22 ± 7	0.48 ± 0.10
$D_s \to \overline{K}^{*0}K^{*+}$	21 ± 5	0.31 ± 0.07
$D_s \to \phi\pi^+\pi^+\pi^-$	10 ± 4	0.39 ± 0.10
$D_s \to \phi\pi^+\pi^0$	18 ± 6	0.39 ± 0.10
$D_s \to \phi\ell^+\nu$	80 ± 16	0.38 ± 0.06

Table 4: *Numbers of* D_s *signal events and fractions of combinatorial background events measured in the different* D_s *decay channels. The level of the combinatorial background has been evaluated inside a mass interval of* $\pm 2\sigma$ (± 1.5,) *centred on the measured* D_s (ϕ) *mass.*

3.4 Selection of the $\phi\ell h$ inclusive channel

Inclusive B_s^0 semileptonic decays are reconstructed by requiring, in the same hemisphere, a high p_T lepton and a reconstructed $\phi \to K^+K^-$. This analysis is expected to be more efficient than analyses based on completely reconstructed D_s^+, at the cost of a higher background. The extra contamination comes mainly from combinatorial K^+K^- pairs and from non-strange B-decays.
In order to avoid a statistical overlap with the $D_s\ell$ sample considered previously, all $K^+K^-\ell$ triplets selected in the $D_s\ell$ channels containing a ϕ in the final state have been excluded from the present sample.
The analysis of the $\phi\ell h$ channel has been performed using 94-95 data only.
Leptons are required to have a momentum and a transverse momentum larger than 3.0 GeV/c and 1.0 GeV/c respectively. A pair of oppositely charged identified kaons is considered as a ϕ candidate provided their combined momentum is above 3.0 GeV/c. Considering the remaining particles of charge opposite to the lepton, the hadron h with the highest momentum projected along the ϕ direction is associated to the D_s^+ decay vertex. The $K^+K^-h^+$ vertex is fitted, and the D_s^+ pseudo-track is reconstructed and fitted with the lepton track to estimate the B decay vertex. The mass distribution of the K^+K^- pairs has been fitted with a Breit-Wigner function to account for true ϕ mesons and a polynomial function for the combinatorial background (Figure 4).
Accepting events within ± 1, of the fitted ϕ mass, where , corresponds to the fitted width of the signal, 441 events are retained, including a combinatorial background of $(45.2 \pm 4.5)\%$.

3.5 Sample composition

The lifetime and the oscillations of B_s^0 mesons have been studied selecting, in the $D_s\ell$ sample, right-sign events lying in a mass interval of $\pm 2\sigma$ (± 1.5,) centered on the measured D_s (ϕ) mass and, in the $\phi\ell h$ sample, events with the candidate ϕ meson in a mass interval of ± 1, centered on the measured ϕ mass.
The following components, entering into the selected sample, have to be considered:

	$\phi\pi$	$\phi\ell$	Others
$f_{bcl}/f_{bl}^{\mathrm{B}_s^0}$	0.151 ± 0.018	0.148 ± 0.025	0.114 ± 0.020

Table 5: *Ratio between* $\mathrm{D_s}\overline{\mathrm{D}}$ *and signal yields in the three* $\mathrm{D_s}\ell$ *classes.*

- f_{bkg}: fraction of candidates from the combinatorial background: it has been evaluated from the fit of the mass distributions on $\mathrm{D_s}\ell$ and $\phi\ell h$ events;
- $f_{f\ell}$: fraction of candidates coming from events having a fake lepton and a real $\mathrm{D_s}$ or ϕ meson (in the $\phi\ell h$ analysis this category includes also events containing true leptons and ϕ mesons coming from charm decays or light quark hadronization);
- $f_{bc\ell}$: fraction of candidates in which the high p_T lepton originates from a "cascade" decay ($b \to c \to \bar{\ell}$);
- $f_{b\ell}^{\mathrm{B}}$: fraction of semileptonic decays of non-strange B mesons
- $f_{b\ell}^{\mathrm{B}_s^0}$: fraction of semileptonic decays of the $\mathrm{B_s^0}$ meson.

Only the last four components (i.e. background and signal coming from physical processes) will be detailed in the following: the estimation of the combinatorial background has been already reported in previous sections.

3.5.1 Composition of the $\mathrm{D_s}\ell$ sample

In the $\mathrm{D_s}\ell$ sample the $\mathrm{D_s}$ signal of the "right" sign correlation is dominated by $\mathrm{B_s^0}$ semileptonic decays; other minor sources of $\mathrm{D_s}\ell$ candidates are:

- $f_{f\ell}$:
  a possible contribution from this source ($\mathrm{D_s^+}$-fake ℓ) would give the same contribution in right and wrong sign candidates. Since no excess has been observed in wrong sign candidates this component has been neglected.
- $f_{bc\ell}$:
  it is the expected fraction of "cascade" decays ($\mathrm{B} \to \overline{\mathrm{D}}^{(\star)}\mathrm{D_s}^{(\star)+}\mathrm{X}$) followed by the semileptonic decay $\overline{\mathrm{D}} \to \ell^-\overline{\nu}\mathrm{X}$ yielding right-sign $\mathrm{D_s^\pm}\ell^\mp$ pairs (referred also as $f_{\mathrm{D_sD}}$). This background corresponds approximately to the same number of events as the signal [20], but the selection efficiency is lower because of the requirement of a high p_T lepton and of a high mass of the($\mathrm{D_s}\ell$) system. These selection criteria reduce the $\mathrm{D_s}\overline{\mathrm{D}}$ background fractions to the values reported in Table 5. Quoted errors on these fractions result from the uncertainties on the branching fractions of the contributing processes and from the errors on the respective experimental selection efficiencies.
- $f_{b\ell}^{\mathrm{B}}$:
  two contributions to this fraction have been considered:
  - f_{refl}: the fraction of events from $\mathrm{D^+} \to \mathrm{K^-}\pi^+\pi^+$ and $\mathrm{D^+} \to \mathrm{K_S^0}\pi^+$ decays in which a π^+ has been misidentified as a $\mathrm{K^+}$ which give candidates in the $\mathrm{D_s}$ mass region. If the $\mathrm{D^+}$ is accompanied by an oppositely charged lepton in the decay $\overline{\mathrm{B}}_{\mathrm{u,d}} \to \mathrm{D^+}\ell^-\overline{\nu}\mathrm{X}$, it looks like a $\overline{\mathrm{B_s^0}}$ semileptonic decay. The fractions $f_{refl}/f_{\mathrm{B_s}} = 0.054 \pm 0.015$ and $f_{refl}/f_{\mathrm{B_s}} = 0.069 \pm 0.025$ have been estimated for the $\overline{\mathrm{K}}^{\star 0}\mathrm{K^+}$ and $\mathrm{K_S^0K^+}$ decay channels, respectively.
  - A $\mathrm{D_s^\pm}\ell^\mp$ pair from a non-strange B meson decay, with the lepton emitted from a direct B semileptonic decay, may come from the decay $\overline{\mathrm{B}} \to \mathrm{D_sKX}\ell^-\overline{\nu}$. The

	$\phi\pi$	$\phi\ell$	$K^0_S K^+$	$K^{*0}K^+$	Others
$f_{B^0_s}$	0.869 ± 0.014	0.871 ± 0.019	0.845 ± 0.023	0.856 ± 0.018	0.898 ± 0.016
$f_{D_s\overline{D}}$	0.131 ± 0.016	0.129 ± 0.022	0.096 ± 0.021	0.098 ± 0.020	0.102 ± 0.018
$f_{refl.}$	-	-	0.059 ± 0.022	0.046 ± 0.014	-

Table 6: Estimated composition of the D_s signal in the $D_s\ell$ sample

production of D_s in B decays not originating from $W^+ \to c\overline{s}$, has been measured by CLEO [21], but no measurement of this production in semileptonic decays exists yet. This process implies the production of a D^{**} followed by its decay into D_sK. This decay is suppressed by phase space (the D_s K system has a large mass) and by the required additional $s\overline{s}$ pair. A detailed calculation shows that the contribution of this process is [22]:

$$\frac{\mathrm{Br}(b \to \overline{B} \to D_s K X \ell^- \overline{\nu})}{\mathrm{Br}(b \to \overline{B^0_s} \to D_s \ell^- \overline{\nu})} < 10\%.$$

Assuming a selection efficiency similar to the one for the $D_s\overline{D}$ component the contribution of this decay channel is below 2% and, for this reason, has been neglected in the following.

Taking into account the above components, the estimated number of B^0_s semileptonic decays in the sample of 436 candidates is 230 ± 18.
The signal composition for each D_s decay mode is given in Table 6.

In order to increase the effective B^0_s purity of the selected sample, signal and background fractions have been calculated on an event by event basis using the probability density functions of $p_T(l)$ and X_{D_s} (defined in Section 3.1):

$$\begin{aligned}
f^{eff}_{bkg} &= f_{bkg}\mathcal{F}_{Comb}(X_{D_s})\mathcal{F}_{Comb}(p_T)/Tot \\
f^{eff}_{B^0_s} &= f_{B^0_s}\mathcal{F}_{D_s}(X_{D_s})\mathcal{F}_{B^0_s}(p_T)/Tot \\
f^{eff}_{D_sD} &= f_{D_sD}\mathcal{F}_{D_s}(X_{D_s})\mathcal{F}_{D_sD}(p_T)/Tot \\
f^{eff}_{refl} &= f_{refl}\mathcal{F}_{D_s}(X_{D_s})\mathcal{F}_{B^0_s}(p_T)/Tot
\end{aligned}$$

where $\mathcal{F}_{D_s}$, $\mathcal{F}_{Comb}$, $\mathcal{F}_{D_sD}$, $\mathcal{F}_{B^0_s}$ are the probability densities for the D_s mesons, the combinatorial background, the D_sD background and the B^0_s signal events, respectively.
In these expressions, Tot is a normalisation factor such that:

$$f^{eff}_{bkg} + f^{eff}_{B^0_s} + f^{eff}_{D_sD} + f^{eff}_{refl} = 1.$$

The distributions of the values of the X_{D_s} and p_T variables are shown in Figure 5. The use of this procedure is equivalent to increasing the statistics by a factor 1.2.

3.5.2 Composition of the $\phi\ell h$ sample

The different contributions to $\phi\ell h$ candidates contained in the selected K^+K^- mass interval of $\pm 6.6\ MeV/c^2$ around the ϕ nominal mass and corresponding to a real ϕ meson are shown in Table 7 and have been estimated using simulated events and measured branching fractions. Quoted uncertainties originate from the finite Monte Carlo statistics,

Source	(%)
$f_{f\ell}$	22.5 ± 2.4
$f_{b\ell}^{\mathrm{B}}$	49.4 ± 2.1
$f_{bc\ell}$	11.3 ± 1.2
$f_{b\ell}^{\mathrm{B_s^0}}$	$16.9^{+6.0}_{-4.3}$

Table 7: *Estimated composition of the ϕ signal in the $\phi\ell h$ sample*

except for one attached to the signal fraction which is dominated by $f_{\mathrm{B_s^0}} \times \mathrm{Br}(\mathrm{B_s^0} \to \mathrm{D_s^+}\ell^-\bar{\nu}_\ell \mathrm{X}) = (0.86 \pm 0.09^{+0.29}_{-0.20})\%$ [23].

The number of $\mathrm{B_s^0}$ semileptonic decays contained in this sample has been evaluated to be 41^{+15}_{-10}.

3.6 Measurement of the B meson decay time

For each event, the $\mathrm{B_s^0}$ decay time is obtained from the measured decay length ($L_{\mathrm{B_s^0}}$) and the estimate of the $\mathrm{B_s^0}$ momentum ($p_{\mathrm{B_s^0}}$). The $\mathrm{B_s^0}$ momentum is estimated using the measured energies:

$$p_{\mathrm{B_s^0}}{}^2 = (E(\mathrm{D_s}\ell) + E_\nu)^2 - m_{\mathrm{B_s^0}}{}^2.$$

The neutrino energy E_ν is obtained from the measured value of E_{miss} (see Section 3.1). The agreement between data and simulation on E_{miss} has been verified using the side bands of the $\mathrm{D_s}\ell$ sample. In order to have enough statistics to perform this test, cuts not correlated with the missing energy have been relaxed. In addition, to verify the resolution on the energy estimate, the studied sample has been enriched in light quark events by applying an anti–b-tagging cut (Section 2.4). A relative shift of $\Delta(MC - Data) = 500\ MeV$ has been measured and the simulation has been corrected. Figure 6 shows the agreement between data and simulation after having applied this correction. The neutrino E_ν resolution has been improved by correcting E_{miss} by a function of ($\mathrm{D_s}\ell$) energy[2] and which has been determined from simulated signal events:

$$E_\nu = E_{miss} + F(E(\mathrm{D_s}\ell)).$$

The data-simulation agreement on $p_{\mathrm{B_s^0}}$ has been verified on the selected signal events after subtraction of the combinatorial background (estimated from events selected in side-bands of $\mathrm{D_s}$ and ϕ signals) (Figure 6).

3.7 Proper time resolution and acceptance

The predicted decay time distributions have been obtained by convoluting the theoretical distributions with resolution functions evaluated from simulated events. Due to different resolutions on the decay length, different parametrizations of the proper time resolution have been used for three different classes in the $\mathrm{D_s}\ell$ sample: $\mathrm{K_S^0 K^+}$ decays, other non-leptonic decays and semileptonic $\mathrm{D_s}$ decays. Different parametrizations have been also used for the two Vertex Detector configurations installed in 91-93 and in 94-95.

[2] here $\mathrm{D_s}$ means "observed decay products of $\mathrm{D_s}$", including also the decays where the $\mathrm{D_s}$ is not fully reconstructed: specifically $\mathrm{D_s^+} \to \phi\ell^+\nu_\ell$ and $\mathrm{D_s^+} \to \phi h^+ X$

The proper time resolution is obtained from the distribution of the difference between the generated (t) and the reconstructed (t_i) time. The following distributions have been considered:

- $\mathcal{R}_{bl}(t-t_i)$ is the resolution function for direct semileptonic B decays.
  $\mathcal{R}_{bl}$ is parametrized, for the $D_s\ell$ sample, as the sum of three Gaussian distributions. The width of the third Gaussian is taken to be proportional to the width of the second Gaussian.

  $$\mathcal{R}_{b\ell}(t-t_i) = (1-f_2-f_3)G(t-t_i,\sigma_1) + f_2 G(t-t_i,\sigma_2) + f_3 G(t-t_i,\sigma_3)$$
  $$\text{with } \sigma_1 = \sqrt{\sigma_{L1}^2 + \sigma_{P1}^2 t^2}$$
  $$\sigma_2 = \sqrt{\sigma_{L2}^2 + \sigma_{P2}^2 t^2}$$
  $$\sigma_3 = s_3 \sigma_2$$

  In the $\phi\ell h$ analysis a fourth Gaussian distribution has been added.
  The parameters related to the decay length and proper time resolutions, σ_{L_i} and σ_{P_i} respectively, and the relative fractions f_i are listed in Table 8. A typical parametrization of the resolution, for the $D_s\ell$ sample, is shown in Figure 7 for the $\phi\pi^+$ decay mode obtained with the 94-95 Vertex-Detector configuration.

- $\mathcal{R}_{bcl}$ is the resolution function applied to "cascade" events.
  Since the charm decay products have been only partially reconstructed in these events, the momentum of the $\overline{B_s^0}$ candidate is underestimated giving a long positive tail in the proper time resolution function.
  The function, $\mathcal{R}_{bcl}(t-t_i)$, is well described by a Gaussian distribution convoluted with an exponential distribution. The variation of the shape of this distribution with the generated proper time has been neglected.

$D_s\ell$ sample							
D_s decay mode	$\sigma_{L1}(ps)$	σ_{P1}	$\sigma_{L2}(ps)$	σ_{P2}	s_3	f_2	f_3
$K_S^0K^+$ (92-93)	0.16	0.08	1.04	0.16	-	0.50	0
$K_S^0K^+$ (94-95)	0.16	0.08	0.98	0.16	-	0.28	0
other non-leptonic (92-93)	0.11	0.07	0.39	0.16	5	0.26	0.07
other non-leptonic (94-95)	0.11	0.07	0.37	0.16	3	0.16	0.02
$\phi\ell^+\nu$ (92-93)	0.14	0.075	0.31	0.15	6	0.29	0.09
$\phi\ell^+\nu$ (94-95)	0.14	0.075	0.31	0.15	6	0.21	0.07

$\phi\ell h$ sample										
$\sigma_{L1}(ps)$	σ_{P1}	$\sigma_{L2}(ps)$	σ_{P2}	$\sigma_{L3}(ps)$	σ_{P3}	$\sigma_{L4}(ps)$	σ_{P4}	f_1	f_2	f_3
0.13	0.08	0.28	0.09	0.32	0.19	1.06	0.42	0.31	0.41	0.10

Table 8: *Fitted values of the parameters of the resolution function $\mathcal{R}_{bl}(t-t_i)$ obtained, on simulated events, for the $D_s\ell$ and $\phi\ell h$ samples.*

Distortions on the reconstructed proper time can be due to a non-uniform reconstruction efficiency as a function of the true proper time (acceptance).

Non-uniform efficiencies have been observed, on simulated events, in the D_s decay modes $\phi\pi$, $K^{*0}K$ and $\phi\ell\nu$ because of the selection criteria on $L/\sigma(L)$.
This effect has been taken into account by inserting in the fitting function, for those channels, an acceptance function ($\mathcal{A}(t)$) parametrized on simulated events.

4 Measurement of the B_s^0 lifetime

The B_s^0 meson lifetime has been studied using the signal sample (Section 3.5) and a background sample containing events selected in the sidebands of D_s (ϕ) candidates. Sidebands events are "right" sign events lying in the D_s mass interval $[1.91 - 1.93] \cup [2.01 - 2.15]$ GeV/c^2 for the D_s hadronic decays and "right" sign events lying in the ϕ mass interval $[0.990, 1.005] \cup [1.035, 1.060]$ GeV/c^2 for the D_s semileptonic decays.
In the $D_s\ell$ analysis "wrong" sign candidates have been also included in the background sample. This background sample is assumed to have the same proper time distribution as the combinatorial background in the signal sample. This assumption has been verified using the simulation. The probability density function used for events in the signal region is given by:

$$P(t_i) = f_{b\ell}^{B_s^0} P_{b\ell}^{B_s^0}(t_i) + f_{b\ell}^{B} P_{b\ell}^{B}(t_i) + f_{bc\ell} P_{bc\ell}(t_i) + f_{f\ell} P_{f\ell}(t_i) + f_{bkg} P_{bkg}(t_i).$$

where t_i and t are the measured and true proper times respectively.
The different probability densities are expressed as convolutions of the physical probability densities with the appropriate resolution ($\mathcal{R}$) and acceptance ($\mathcal{A}$) functions:

- for the signal:

$$P_{b\ell}^{B_s^0}(t_i) = \frac{1}{\tau_{B_s^0}} exp(-t/\tau_{B_s^0}) \mathcal{A}(t) \otimes \mathcal{R}_{b\ell}(t - t_i)$$

- for the background coming from non strange B mesons:

$$P_{b\ell}^{B}(t_i) = \sum_{q \neq s} f_{b\ell}^{B_q} \frac{1}{\tau_{B_q}} exp(-t/\tau_{B_q}) \mathcal{A}(t) \otimes \mathcal{R}_{b\ell}(t - t_i)$$

  where q runs over the various B-hadrons species contributing to this background,
- for the "cascade" background:

$$P_{bc\ell}(t_i) = \sum_{q} f_{bc\ell}^{B_q} \frac{1}{\tau_{B_q}} exp(-t/\tau_{B_q}) \mathcal{A}(t) \otimes \mathcal{R}_{bc\ell}(t - t_i)$$

- for "fake lepton" candidates the function $P_{f\ell}(t_i)$ has been parametrized using simulated events;
- for the combinatorial background two different parametrizations have been used:
  - $D_s\ell$ sample.

$$\begin{aligned} P_{bkg}^{j}(t_i) = \; & f^- \tfrac{1}{\tau^-} exp(-t/\tau^-) \otimes G(t - t_i, \sigma_j) + f^+ \tfrac{1}{\tau^+} exp(-t/\tau^+) \otimes G(t - t_i, \sigma_j) + \\ & (1 - f^- - f^+) G(t - t_i, \sigma_j) \end{aligned}$$

    Three distributions have been used for each of the three classes of decay time resolution σ_j ($j = 1, 3$) (see Section 3.7). A negative exponential for poorly

measured events (with negative lifetime τ^-), an exponential distribution for the flying background (with lifetime τ^+) and a central Gaussian for the non-flying one. The seven parameters (f^-, f^+, τ^+, τ^- and σ_j $(j = 1,3)$) have been fitted independently for the 92-93 and 94-95 data samples. The parameter σ_j $(j = 1,3)$ are taken to be different for the three classes of decay time resolution.

– $\phi\ell h$ sample.
The combinatorial background shape has been described with a sum of four smeared exponentials $(exp(t_i,\tau) \otimes G(t - t_i,\sigma))$.

B_s^0 lifetime fit has been performed simultaneously on the signal and background samples. All parameters describing the shape of the background time distributions in the $D_s\ell$ and $\phi\ell h$ samples are left as free parameters. Results of the fit are shown in Figure 8 ($D_s\ell$ sample) and in Figure 9 ($\phi\ell h$ sample). Table 9 summarizes the different lifetimes measurements with their statistical errors.

Decay mode	Data set	$\tau_{B_s^0}(ps)$
$D_s\ell; D_s \to \phi\pi$	(92-95)	$1.44^{+0.26}_{-0.21}$
$D_s\ell; D_s \to \overline{K}^{*0}K^+$	(92-95)	$1.31^{+0.30}_{-0.25}$
$D_s\ell; D_s \to K_S^0K^+$	(92-95)	$1.43^{+0.61}_{-0.44}$
$D_s\ell; D_s \to \overline{K}^{*0}K^{*+}$	(94-95)	$1.00^{+0.50}_{-0.31}$
$D_s\ell; D_s \to \phi\pi^+\pi^0$	(94-95)	$1.46^{+0.61}_{-0.42}$
$D_s\ell; D_s \to \phi\pi^+\pi^+\pi^-$	(94-95)	$1.96^{+1.16}_{-0.64}$
$D_s\ell; D_s \to \phi\ell^+\nu$	(92-95)	$1.49^{+0.34}_{-0.27}$
$\phi\ell h$	(94-95)	1.41 ± 0.68

Table 9: B_s^0 *lifetime determinations using the* $D_s\ell$ *and* $\phi\ell h$ *events samples.*

4.1 Systematic errors on the B_s^0 lifetime

Systematic uncertainties attached to the B_s^0 lifetime determination are summarized in Table 10.

The main contributions to the systematic uncertainties come from:

- Systematics from the evaluation of the B_s^0 purity.

  – $D_s\ell$ sample:
  The different fractions for signal and background events have been calculated on an event by event basis. The expressions defining the effective purities are given in Section 3.5.1. The value of $f_{bkg.}$ has been varied according to the statistical uncertainties of the fitted combinatorial background fractions present in the different, D_s or K^+K^-, mass distributions. The value of $f_{bc\ell}$ has been varied according to the errors given in Table 7 and in Table 6, which takes into account both the statistical error from the simulation and the errors on measured branching ratios.
  The evaluation of the systematics due to the procedure used to evaluate the

Systematics	$\tau_{B_s^0}$ variation in ps
$f_{bkg.}$	$^{+0.0090}_{-0.0130}$
$f_{bc\ell}$	$^{-0.0100}_{+0.0110}$
$f^{B}_{b\ell}$	$^{-0.0020}_{+0.0020}$
X_{D_s} discrim. var.	$+0.008$
p_T discrim. var.	± 0.004
$\tau_{B^+}(1.65 \pm 0.04\ ps)$	$^{-0.0010}_{+0.0010}$
$\tau_{B_d^0}(1.56 \pm 0.04\ ps)$	$^{-0.0012}_{+0.0013}$
t resolution	± 0.008
t acceptance	± 0.010
Simulated evts. statistics	± 0.020
Total Syst.	± 0.03

Table 10: *Different contributions to the systematic uncertainty attached to the* B_s^0 *lifetime measurement.*

B_s^0 purity on a event by event basis has been evaluated in two steps. The distributions of the variable X_{D_s} (Figure 5) for signal and background events have been re-weighted with as linear function in order to maximize the Data-simulation agreement:

$$\frac{S(X_{D_s})}{B(X_{D_s})}_{\text{new}} = \frac{S(X_{D_s})}{B(X_{D_s})}_{\text{old}} (a + bX_{D_s})$$

The linear behaviour of the correction has been chosen because of the limited statistics in the data: it has been verified that a quadratic correction does not change the result significantly.
The fit has been redone with this new probability distribution and the variation of the fitted lifetime value ($+0.008\ ps$) has been taken as the systematic error.
Because of the agreement between data and simulation (Figure 5-e and 5-f) for the p_T distribution, the systematic error associated to this variable has been evaluated varying its distributions by the uncertainties of the parametrization obtained from simulated events.

– $\phi\ell h$ sample:
In this analysis the fractions of signal and background events have not been calculated on an event by event basis. The systematic uncertainty due to the variation of the $f_{bc\ell}$, $f^B_{b\ell}$ and f_{bkg} fractions have been obtained by varying these parameters by the errors reported in Table 7 and in Table 4. The systematic uncertainty attached to the $f_{f\ell}$ fraction, affecting only the $\phi\ell$ sample, has a negligible effect on the global result.

- Validation of the fitting procedure using simulated events.
The fitting method has been verified on pure B_s^0 simulated events: the measured value on this sample has been $\tau_{B_s^0}(D_s^{\pm}\ell^{\mp})^{\text{MC}} = (1.605 \pm 0.020)$ps in agreement with the generated value ($\tau_{B_s^0} = 1.6\ ps$). The statistical error of this verification has been included in the systematic uncertainties.
A similar check has been performed on the $\phi\ell h$ sample giving $\tau_{B_s^0}(\phi\ell\text{h})^{\text{MC}} =$

(1.65 ± 0.04)ps. Since the statistical weight of the $\phi\ell h$ channel is small compared to the full sample, the error on the fitting procedure is dominated by the statistics of $D_s\ell$ simulated events.

- Systematic from the proper time resolution.
  Uncertainties on the determination of the resolution on the proper time receive two contributions: one from errors on the decay distance evaluation and the other from errors on the measurement of the B_s^0 momentum. The agreement between real and simulated events on the evaluation of the errors on the decay distance has been verified by comparing the widths of the negative part of the flight distance distributions, for events which are depleted in B-hadrons. The difference between the two widths has been found to be of the order of 10%.
  The systematic on B_s^0 momentum has been evaluated by comparing the momentum distribution on simulated events with the distribution, background subtracted, obtained from the data sample (see Section 3.5.1). Effects from shift and width differences between the two distributions have been considered by changing the shape of the distribution of simulated events; it has been found that the main systematics comes from difference in width: the width on data has been estimated to be larger by a factor 1.07 ± 0.04.
  Taking into account these two effects the uncertainty on the time resolution has been, conservatively, evaluated by varying the parameters σ_{L_i} and σ_{P_i} of the resolution functions (see Table 8) by $\pm 10\%$.
  Uncertainties on the acceptance determination have been also considered: the parameters entering in the definition of the acceptance function have been varied according to the errors given by the fit on simulated events.

The final result is:

$$\tau_{B_s^0} = 1.42^{+0.14}_{-0.13}(stat.) \pm 0.03(syst.)\ ps. \tag{8}$$

5 Lifetime difference between B_s^0 mass eigenstates

The B_s^0 (or $\overline{B_s^0}$) mesons are superpositions of the two mass eigenstates:

$$|B_s^0\rangle = \frac{1}{\sqrt{2}}(|B_H^0\rangle + |B_L^0\rangle) \quad ; \quad |\overline{B}_s^0\rangle = \frac{1}{\sqrt{2}}(|B_H^0\rangle - |B_L^0\rangle).$$

The probability density for N semileptonic B_s^0 decays is proportional to:

$$\frac{dN}{dt} \propto (\mathrm{Br}(B_H^0 \to \ell X), {}_H e^{-,{}_H t} + \mathrm{Br}(B_L^0 \to \ell X), {}_L e^{-,{}_L t}) \tag{9}$$

where $\mathrm{Br}(B^0_{H(L)} \to \ell X) = , (B^0_{H(L)} \to \ell X)/, {}_{H(L)}$.
The semileptonic partial widths for B_H^0 and B_L^0 are assumed to be equal since only CP-eigenstates could generate a difference (semileptonic decays are not CP-eigenstates).
It follows that the two exponentials are multiplied by the same factor and the probability density for the decay of a B_s^0 or $\overline{B_s^0}$ at time t is given, after normalization, by:

$$\mathcal{P}(t) = \frac{, {}_H, {}_L}{, {}_H + , {}_L}\ (e^{-,{}_H t} + e^{-,{}_L t}) \tag{10}$$

where $, {}_L = , {}_{B_s^0} + \Delta, {}_{B_s^0}/2$, $, {}_H = , {}_{B_s^0} - \Delta, {}_{B_s^0}/2$.

Two independent variables are then considered: $\tau \equiv 1/,_{\mathrm{B_s^0}}$[3] and $\delta \equiv \Delta,_{\mathrm{B_s^0}}/,_{\mathrm{B_s^0}}$.
As the statistics in the sample is not sufficient to fit simultaneously τ and δ, the method used to evaluate δ consists in calculating the log-likelihood for the time distribution measured with the $\mathrm{D_s}\ell$ and $\phi\ell h$ samples and deriving the probability density function for δ by constraining τ to be equal to $1/,_{\mathrm{B_d^0}} \equiv \tau_{\mathrm{B_d}} = (1.56 \pm 0.04)$ ps [19][4] ($|,_{\mathrm{B_s}}/,_{\mathrm{B_d}} - 1| < 0.01$ is predicted in [1]).

The log-likelihoods function described in Section 4 have been modified by replacing the physical function $\mathrm{B_s^0}$ $(\exp(-t/\tau_{\mathrm{B_s^0}}))$ by Equation (10) and they have been added.
The log-likelihood sum has been minimized in the (τ, δ) plane and the difference with respect to its minimum ($\Delta\mathcal{L}$) has been calculated (Figure 10-a):

$$\Delta\mathcal{L} = -\log \mathcal{L}_{tot}^{\mathrm{D_s}\ell+\phi\ell h}(\tau,\delta) + \log \mathcal{L}_{tot}^{\mathrm{D_s}\ell+\phi\ell h}((\tau)^{min},(\delta)^{min}) \; .$$

The probability density function for the variables τ and δ is then proportional to:

$$\mathcal{P}(\tau,\delta) \propto e^{-\Delta\mathcal{L}}$$

The δ probability distribution is obtained by convoluting $\mathcal{P}(\tau,\delta)$ with the probability density function $f_{(\tau=\tau_{\mathrm{B_d^0}})}(\tau)$, expressing the constraint $\tau = \tau_{\mathrm{B_d^0}}$, and normalizing the result:

$$\mathcal{P}(\delta) = \frac{\int \mathcal{P}(\tau,\delta) f_{(\tau=\tau_{\mathrm{B_d^0}})}(\tau) d\tau}{\int \mathcal{P}(\tau,\delta) f_{(\tau=\tau_{\mathrm{B_d^0}})}(\tau) d\tau d\delta}$$

where

$$f_{(\tau=\tau_{\mathrm{B_d^0}})}(\tau) = 1/(\sqrt{2\pi}\sigma_{\tau_{\mathrm{B_d^0}}}) \exp(-(\tau-\tau_{\mathrm{B_d^0}})^2/2\sigma^2_{\tau_{\mathrm{B_d^0}}})$$

The upper limit on $\Delta,_{\mathrm{B_s^0}}/,_{\mathrm{B_s^0}}$, calculated from $\mathcal{P}(\delta)$, is:

$$\Delta,_{\mathrm{B_s^0}}/,_{\mathrm{B_s^0}} < 0.45 \text{ at the } 95\% \text{ C.L.}$$

This limit takes into account both statistical uncertainties and the systematic coming from the uncertainty on the $\mathrm{B_d^0}$ lifetime.
The systematic uncertainty originating from other sources has been evaluated by convoluting $\mathcal{P}(\tau,\delta)$ with the probability density functions of the corresponding parameters:

$$\mathcal{P}(\delta) = \frac{\int \mathcal{P}(\tau,\delta,x^1_{sys},...,x^n_{sys}) f_{(\tau=\tau_{\mathrm{B_d^0}})}(\tau) f(x^1_{sys})...f_(x^n_{sys}) d\tau dx^1_{sys}...dx^n_{sys}}{\int \mathcal{P}(\tau,\delta,x^1_{sys},...,x^n_{sys}) f_{(\tau=\tau_{\mathrm{B_d^0}})}(\tau) f(x^1_{sys})...f_(x^n_{sys}) d\tau dx^1_{sys}...dx^n_{sys} d\delta}$$

where x^i_{sys} are the n parameters considered in the systematic uncertainty and $f(x^i_{sys})$ are the corresponding probability densities.
Since the method implies heavy numerical integrations over a n-dimensional grid only two systematics have been considered here: the purity in $\mathrm{B_s^0}$ meson of the selected sample and the acceptance. This approximation is justified since systematic uncertainties are expected to be small (as they are in the lifetime measurement) and dominated by these two parameters.
The $\Delta,_{\mathrm{B_s^0}}/,_{\mathrm{B_s^0}}$ probability distribution, obtained with the inclusion of the systematics, is shown in Figure 10-c, the most probable value for $\Delta,_{\mathrm{B_s^0}}/,_{\mathrm{B_s^0}}$ is 0 and the upper limit at 95% confidence level is:

$$\Delta,_{\mathrm{B_s^0}}/,_{\mathrm{B_s^0}} < 0.46 \text{ at the } 95\% \text{ C.L.}$$

[3] τ does not coincide with the measured $\mathrm{B_s^0}$ lifetime if $\Delta,_{\mathrm{B_s^0}}$ is different from zero

[4] It has been assumed that $\Delta,_{\mathrm{B_d}} = 0$.

It should be noted that the world average of the B_s^0 lifetime cannot be used as constraint in such analysis, since it depends on Δ, $_{B_s^0}$ and on , $_{B_s^0}$. Moreover, this dependence is also different for different decay channels. In the $D_s\ell$ case the expression of the average B_s^0 lifetime is given by:

$$\tau_{B_s^0}(D_s\ell) = \frac{1 + (\frac{1}{2}\Delta, _{B_s^0}/, _{B_s^0})^2}{, _{B_s^0}(1 - (\frac{1}{2}\Delta, _{B_s^0}/, _{B_s^0})^2)} \tag{11}$$

6 Study of B_s^0-$\overline{B_s^0}$ oscillations

The study of B_s^0-$\overline{B_s^0}$ oscillations requires the tagging of the sign of the b quark in the B_s^0 meson at the decay and production times.
The algorithm used for the $b(\overline{b})$ tagging at production time has been tuned in order to have the best performances on the $D_s\ell$ sample, where all the charged particles from the B_s^0 decays have been reconstructed.

6.1 $b(\overline{b})$ tagging at production time

The signature of the initial production of a $b(\overline{b})$ quark in the jet containing the B_s^0 or $\overline{B_s^0}$ candidate is determined using a combination of different variables which are sensitive to the initial quark state following the same technique as in Section 3.1. For each individual variable X_i, the probability density functions $f_b(X_i)$ ($f_{\overline{b}}(X_i)$) for b ($\overline{b}$) quarks are obtained from the simulation and the ratio $R_i = f_{\overline{b}}(X_i)/f_b(X_i)$ is computed. The combined tagging variable is defined as:

$$x_{tag} = \frac{1 - R}{1 + R}, \text{ where } R = \prod R_i. \tag{12}$$

The variable x_{tag} varies between -1 and 1. High values of x_{tag} correspond to a high probability that a given hemisphere contains a b quark in the initial state. If some of the variables X_i are not defined in a given event, the corresponding ratios R_i are set to 1, corresponding to equal probabilities for the initial state to be b or $\overline{b}$.
An event is split into two hemispheres by the plane passing through the beam interaction point and perpendicular to the direction of the B_s^0 candidate; then nine discriminant variables have been selected for this analysis. Five variables are defined in the hemisphere opposite to the B_s^0 meson, in which reconstructed charged particles have been used:

- the mean hemisphere charge which is defined as :

$$Q_{hem} = \frac{\sum_{i=1}^{n} q_i(|\vec{p_i} \cdot \vec{e_s}|)^\kappa}{\sum_{i=1}^{n}(|\vec{p_i} \cdot \vec{e_s}|)^\kappa}. \tag{13}$$

  In this expression n is total number of charged particles in the hemisphere, q_i and $\vec{p_i}$ are, respectively, the charge and the momentum of particle i $\vec{e_s}$ is the unit vector along the thrust axis and κ=0.6;
- the weighted sum of the charges of particles with tracks identified as kaon candidates:

$$Q_K = \sum q_i(|\vec{p_i} \cdot \vec{e_s}|)^\kappa;$$

- the sum of the charges of tracks having significant impact parameters with respect to the event primary vertex;

- the sum of the charges of the particles whose tracks are compatible with the event primary vertex;
- the momentum transverse to the jet axis multiplied by the charge of the identified lepton candidate with the highest momentum.

These variables have been combined to form the discriminant variable x^o_{tag}.

Another set of three variables are evaluated in the hemisphere which contains the B^0_s meson candidate and only tracks not included in the B^0_s candidate decay products have been used in their determination [5]. They are:

- the mean hemisphere charge, computed using (13) with $\vec{e_s}$ directed along the reconstructed momentum of the B^0_s candidate;
- the rapidity with respect to the direction of the thrust axis multiplied by the charge of the identified kaon candidate with the highest momentum having a trajectory compatible with the primary vertex (this algorithm aims at reconstructing the fragmentation kaon produced with the $\overline{B^0_s}$, this kaon has a sign opposite to the b quark contained in the meson);
- the momentum of any reconstructed Λ^0 candidate multiplied by the charge of the proton from its decay (same principle as in the previous item when a baryon instead of meson is produced).

These variables have been combined to form the discriminant variable x^s_{tag}. In addition the distribution of the polar angle of the direction of the thrust axis, common to both hemispheres, is also used to benefit from the forward-backward asymmetry of the b quark production relative to the electron beam axis.

6.2 Measurement of the tagging purity in events with an exclusively reconstructed D^*

The high statistics sample of exclusively reconstructed D^*, accumulated in 1994-95, has been used to check the tagging procedure. The purity of the tagging at production time, ϵ_{tag}, has been measured on those events using the analysis of the $B^0_d - \overline{B^0_d}$ mixing.

The $D^{*\pm}$ candidates have been selected by reconstructing the decay chain $D^{*+} \to D^0\pi^+$ followed by $D^0 \to K^-\pi^+$ or $D^0 \to K^-\pi^+\pi^0$. The selection criteria rely mainly on the small mass difference between D^{*+} and D^0 mesons [24]. The measurement of the $B^0_d - \overline{B^0_d}$ mixing is performed by correlating *a)* the sign of the $D^{*\pm}$ charge, which tags the B flavour at decay time (since D^{*-} in these events are mainly produced from B^0_d and D^{*+} from $\overline{B^0_d}$), with *b)* the global tagging variable, x^o_{tag}, evaluated in the hemisphere opposite to the $D^{*\pm}$ and obtained by combining the five first quantities defined in the previous section. If the B^0_d meson, decaying into a $D^{*\pm}$, has oscillated, the $D^{*\pm}$ charge and the value of the variable x^o_{tag} are expected to be of unlike sign. The mass difference, $\Delta m_{B^0_d}$, between the two physical states of the $B^0_d - \overline{B^0_d}$ system is obtained from the study of the D^0 decay distance distribution for unlike and like sign events. Details of the analysis can be found in [24]. The amplitude of the time dependent oscillation is sensitive to the probability of correctly tagging events as unmixed and mixed B^0_d candidates. A fit has been performed, fixing the mass difference $\Delta m_{B^0_d}$ to the world average [23], and leaving ϵ_{tag} as a free parameter. The fit has been repeated for different minimum values of the global tagging

[5] In the $D_s\ell$ analysis all the B^0_s decay products are identified and removed, for more inclusive analyses this is only partially possible

variable x^o_{tag}. Results are reported in Table 11, together with the predictions from the simulation. The fraction of events f_{events} remaining after the cut on the tagging variable is also reported.

	Data		Simulation	
	ϵ_{tag}	f_{events}	ϵ_{tag}	f_{events}
$\|x^o_{tag}\| > 0.0$	0.68 ± 0.02	1.0	0.69	1.0
$\|x^o_{tag}\| > 0.1$	0.69 ± 0.02	0.88	0.71	0.89
$\|x^o_{tag}\| > 0.2$	0.71 ± 0.02	0.77	0.74	0.78

Table 11: *Values of ϵ_{tag} obtained from the analysis of exclusively reconstructed $D^{*\pm}$ for different cuts on the value of the tagging variable x^o_{tag}. Also reported is the fraction of events remaining after the cut. Expectations from the simulation are also given.*

The tagging efficiency, estimated using the $D^{*\pm}$ sample, is consistent within its uncertainty with the expectation from the simulation.

The selected sample of exclusively reconstructed $D^{*\pm}$ still contains a significant fraction of events originating from charm and light quarks. In order to study the distribution of the tagging variable x^o_{tag}, the b-tag probability for all tracks in the event has been required to be smaller than 10^{-3} [16]. The fraction of non-b events in the remaining sample is estimated to be 5%. The distribution of the product between the $D^{*\pm}$ charge and the value of the tagging variable x^o_{tag} is shown in Figure 11–a, together with the expectation from the simulation.

Another check has been performed by selecting events with an exclusively reconstructed $D^{*\pm}$ accompanied by a lepton of opposite charge. This sample is highly enriched in B^0_d, but has a limited statistics. However, it allows the study of the tagging variable x^s_{tag} defined, in the same hemisphere as the $D^{*\pm}$-lepton candidate, by combining the other three variables mentioned in the previous section. The variable which quantifies the presence of an identified kaon of highest momentum compatible with the primary vertex has been removed from the definition of x^s_{tag}. The distribution of the product between the $D^{*\pm}$ charge and the value of the tagging variable, x^s_{tag}, is shown in Figure 11–b together with the expectation from the simulation.

The selected $D_s\ell$ sample do not have enough statistics to perform a quantitative check. The x_{tag} distributions expected from the simulation and measured data, using the $D_s\ell$ sample, are found to be compatible within statistics (Figure 12).

6.3 Tagging procedure

An event is classified as a mixed or an unmixed candidate according to the relative signs of the D_s electric charge, Q_D, and of the x_{tag} variable. Mixed candidates have $x_{tag} \times Q_D < 0$, and unmixed ones $x_{tag} \times Q_D > 0$.

The probability, ϵ_b, of tagging the b or the $\overline{b}$ quark correctly from the measurement of x_{tag} has been evaluated using a dedicated simulated event sample and has been found to be, in the $D_s\ell$ sample, $74.5 \pm 0.5\%$ in 94-95 data and $71.5 \pm 1.2\%$ in 92-93 data.

In the $\phi\ell h$ sample the tracks from the B decay have not been all reconstructed. The tagging purity is lower with respect to the one estimated in the $D_s\ell$ sample due to some possible misidentification between primary and secondary tracks present in the same hemisphere as the ϕ meson. The value found in simulated events is ($\epsilon_b = 0.69 \pm 0.01$).

To improve the tagging purity further, the shape of the x_{tag} distribution can be included in the analysis.
Four purities enter in the analysis:

- $\epsilon_{b\ell}$: tagging purity for the direct $b \to \ell$ decays;
- $\epsilon_{bc\ell}$: tagging purity for $b \to c \to \ell$ "cascade" decays;
- $\epsilon_{bkg}^{mix(unmix)}$ probability of classifying background candidates as mixed or as unmixed (computed on sidebands events);
- $\epsilon_{f\ell}^{mix(unmix)}$ probability of classifying fake lepton candidates as mixed or as unmixed.

using x_{tag} as a discriminant variable each of these purities is replaced by the function $\epsilon X(x_{tag})$, where X is the x_{tag} probability density function.
The global probability density function has been divided by the sum $\epsilon X^r_{b\ell}(x_{tag}) + (1-\epsilon)X^w_{b\ell}(x_{tag})$ ($r \equiv$ right tag and $w \equiv$ wrong tag) in order to keep, for the signal part, the relation $\epsilon^w = 1 - \epsilon^r$.
The functions entering in the final likelihood are then re-defined as:

$$X^r_{b\ell} = \frac{\epsilon_{b\ell} X^r_{b\ell}(x_{tag})}{\epsilon_{b\ell} X^r_{b\ell}(x_{tag}) + (1-\epsilon_{b\ell}) X^w_{b\ell}(x_{tag})} \qquad X^w_{b\ell} = 1 - X^r_{b\ell}$$

$$X^r_{bc\ell} = \frac{\epsilon_{bc\ell} X^r_{bc\ell}}{\epsilon_{b\ell} X^r_{b\ell}(x_{tag}) + (1-\epsilon_{b\ell}) X^w_{b\ell}(x_{tag})} \qquad X^w_{bc\ell} = \frac{(1-\epsilon_{bc\ell}) X^w_{bc\ell}}{\epsilon_{b\ell} X^r_{b\ell}(x_{tag}) + (1-\epsilon_{b\ell}) X^w_{b\ell}(x_{tag})}$$

$$X^{mix}_{bkg} = \frac{\epsilon^{mix}_{bkg} X^{mix}_{bkg}}{\epsilon_{b\ell} X^r_{b\ell}(x_{tag}) + (1-\epsilon_{b\ell}) X^w_{b\ell}(x_{tag})} \qquad X^{unmix}_{bkg} = \frac{\epsilon^{unmix}_{bkg} X^{unmix}_{bkg}}{\epsilon_{b\ell} X^r_{b\ell}(x_{tag}) + (1-\epsilon_{b\ell}) X^w_{b\ell}(x_{tag})}$$

$$X^{mix}_{f\ell} = \frac{\epsilon^{mix}_{f\ell} X^{mix}_{f\ell}}{\epsilon_{b\ell} X^r_{b\ell}(x_{tag}) + (1-\epsilon_{b\ell}) X^w_{b\ell}(x_{tag})} \qquad X^{unmix}_{f\ell} = \frac{\epsilon^{unmix}_{f\ell} X^{unmix}_{f\ell}}{\epsilon_{b\ell} X^r_{b\ell}(x_{tag}) + (1-\epsilon_{b\ell}) X^w_{b\ell}(x_{tag})}$$

The effective tagging purities obtained, in the $D_s\ell$ sample, with this method correspond to $78 \pm 0.5\%$ for 94-95 data and to $74 \pm 1.2\%$ for 92-93 data.

6.4 Fitting procedure

From the expected proper time distributions and the tagging probabilities, the probability functions for mixed and unmixed events candidates have been computed [6]:

$$P^{mix}(t_i) = f^{B^0_s}_{b\ell} P^{mix}_{B^0_s}(t_i) + f^{B}_{b\ell} P^{mix}_{B}(t_i) + f_{bc\ell} P^{mix}_{bc\ell}(t_i) + f_{f\ell} P^{mix}_{f\ell}(t_i) + f_{bkg} P^{mix}_{bkg}(t_i). \quad (14)$$

where t_i is the reconstructed proper time. The analytical probability densities are as follows, with t being the true proper time:

- B^0_s mixing probability.

$$P^{mix}_{B^0_s}(t_i) \;\; = \{ \;\; X^r_{b\ell} \mathcal{P}^{mix}_{B^0_s}(t) + X^w_{b\ell} \mathcal{P}^{unmix}_{B^0_s}(t) \;\; \} \mathcal{A}(t) \otimes \mathcal{R}_{b\ell}(t - t_i) \quad (15)$$

- "cascade" background mixing probability.

$$\begin{aligned} P^{mix}_{bc\ell}(t_i) = \{ \quad & f^{B_d}_{bc\ell} (\; X^r_{bc\ell} \mathcal{P}^{unmix}_{B_d}(t) + (\; X^w_{bc\ell} \mathcal{P}^{mix}_{B_d}(t) \;) + \\ & (f^{B^0_s}_{bc\ell}/2)(\; X^r_{bc\ell} \mathcal{P}^{unmix}_{B^0_s}(t) + X^w_{bc\ell} \mathcal{P}^{mix}_{B^0_s}(t) \;) + \\ & (f^{B^0_s}_{bc\ell}/2)(\; X^w_{bc\ell} \mathcal{P}^{unmix}_{B^0_s}(t) + X^r_{bc\ell} \mathcal{P}^{mix}_{B^0_s}(t) \;) + \\ & f^{B^+}_{bc\ell} X^r_{bc\ell}/\tau_{B^+} \exp(-t/\tau_{B^+}) \\ & f^{\Lambda_b}_{bc\ell} X^r_{bc\ell}/\tau_{\Lambda_b} \exp(-t/\tau_{\Lambda_b}) \qquad \} \mathcal{A}(t) \otimes \mathcal{R}_{bc\ell}(t - t_i) \end{aligned} \quad (16)$$

[6] In the following, only the probability function for mixed events is written explicitly; the corresponding probability for unmixed events can be obtained by changing $r \to w$.

Note that the two terms contributing to the B_s^0 are due to the fact that, in the decay $B_s^0 \to D_s^+ D_s^- X$, the lepton can originate from either D_s mesons. The B_s^0 contribution can then be simplified in the expression and becomes, mixing independent:

$$f_{B_s^0}/\tau_{B_s^0} \exp(-t/\tau_{B_s^0})$$

- non-strange B-hadrons mixing probability.

$$\begin{aligned} P_{b\ell}^{B\ mix}(t_i) = \{ \quad & f_{b\ell}^{B_d}(\ X_{b\ell}^r \mathcal{P}_{B_d}^{mix}(t) + X_{b\ell}^w \mathcal{P}_{B_d}^{unmix}(t) \ ) + \\ & f_{b\ell}^{B^+} X_{b\ell}^w/\tau_{B^+} \exp(-t/\tau_{B^+}) \\ & f_{b\ell}^{\Lambda_b} X_{b\ell}^w/\tau_{\Lambda_b} \exp(-t/\tau_{\Lambda_b}) \qquad \} \mathcal{A}(t) \otimes \mathcal{R}_{b\ell}(t - t_i) \end{aligned} \tag{17}$$

- mixing probability for candidates from light quark events or fake leptons:

$$P_{f\ell}^{mix}(t_i) = X_{f\ell}^{mix} \mathcal{P}_{f\ell}(t_i) \tag{18}$$

- combinatorial background mixing probability:

$$P_{bkg}^{mix}(t_i) = X_{bkg}^{mix} \mathcal{P}_{bkg}(t_i) \tag{19}$$

The parameters entering in the proper time distribution for this background have been determined in the lifetime fit.

The oscillation analysis has been performed in the framework of the amplitude method [25] which consists in measuring, for each value of the frequency $\Delta m_{B_s^0}$, an amplitude A and its error $\sigma(A)$. The parameter A is introduced in the time evolution of pure B_s^0 or $\overline{B_s^0}$ states so that the value $A = 1$ corresponds to a genuine signal for oscillation:

$$\mathcal{P}(B_s^0 \to (B_s^0,\ \overline{B_s^0})) \ = \ \frac{1}{2\tau_s} e^{-\frac{t}{\tau_s}} \times (1 \pm A \ cos(\Delta m_{B_s^0} t))$$

The 95% C.L. excluded region for $\Delta m_{B_s^0}$ is obtained by evaluating the probability that, in at most 5% of the cases, a real signal having an amplitude equal to unity would give an observed amplitude smaller than the one measured. This corresponds to the condition:

$$A(\Delta m_{B_s^0}) + 1.645 \ \sigma(A(\Delta m_{B_s^0})) \ < \ 1.$$

In the amplitude approach it is possible to define the exclusion probability, that is the probability that a certain $\Delta m_{B_s^0}$ value lies in an excluded region if the generated $\Delta m_{B_s^0}$ was very large ($\Delta m_{B_s^0} \to \infty$). The sensitivity is the value of $\Delta m_{B_s^0}$ corresponding to 50 % of exclusion probability.

Using the amplitude approach (Figure 13), and considering only statistical uncertainties, a limit has been obtained:

$$\Delta m_{B_s^0} > 7.4 \text{ ps}^{-1} \text{ at } 95\% \text{ C.L.} \tag{20}$$

with a corresponding sensitivity at $\Delta m_{B_s^0} = 8.3$ ps^{-1}. At $\Delta m_{B_s^0} = 10\ ps^{-1}$, the error on the amplitude is 0.85.

Several checks have been done to verify the reliability of the amplitude fit: the proper time distributions for mixed and unmixed events have been verified to be well reproduced by the fit (Figure 14-a,-b) and the ratio between mixed events and the total number of events in bins of the proper time has been compared with the expected distribution for

$\Delta m_{B_s^0} = 5\ ps^{-1}$ and $\Delta m_{B_s^0} = 10\ ps^{-1}$. These values have been chosen to illustrate the behaviour of the expected oscillation curve for $A = 0$ ($\Delta m_{B_s^0} = 5\ ps^{-1}$) and $A = 1$ ($\Delta m_{B_s^0} = 10\ ps^{-1}$) (Figure 14-e). It could be seen that the oscillation curve at $\Delta m_{B_s^0} = 10\ ps^{-1}$ (where A is close to 1) fits the data better than the corresponding curve at $\Delta m_{B_s^0} = 5\ ps^{-1}$ (where A is compatible with 0), as expected from the definition of A.

6.5 Study of systematic uncertainties

Systematic uncertainties have been evaluated by varying the parameters which have been kept constant in the fit, according to their measured or expected errors, using the formula [25]:

$$\sigma\left[A(\nu)\right]_{sys} = \Delta A(\nu) + (1 - A)\frac{\Delta\sigma(A)}{\sigma\left[A(\nu)\right]}.$$

$\Delta A(\nu)$ and $\Delta\sigma(A)$ indicate the variations of the amplitude, in the central value and in the error, due to the considered systematics.
Three main sources of systematic uncertainties have been identified:

- Systematics from the tagging purity.
  - $D_s\ell$ sample.
    The studies done in Section 6.2 show that, using the tagging variables in the opposite hemisphere and requiring $|x^o_{tag}| > 0.$, the difference between the values of the tagging purity measured in real and simulated events is $\epsilon_{tag}(DATA) - \epsilon_{tag}(MC)$ = -0.01 $\pm$ 0.02. It has been verified that the real and the simulated distributions for the tagging purities agree in both hemispheres. The systematics coming from the control of the tagging purity has been evaluated by varying the probability distributions of the discriminant variable for b and $\overline{b}$ quarks in a way to induce an absolute variation on the effective value of the tagging purity of $\pm$3.0%.

  - $\phi\ell h$ sample. The agreement between data and simulation has not been checked for this sample; a conservative absolute variation of 5% in the tagging purity has been assumed.
- Systematics from the B_s^0 purity.
  The same procedure already applied for the lifetime measurement has been used.
- Systematics from the resolution on the B decay proper time.
  The same procedure already applied for the lifetime measurement has been used. In addition, the systematic error due to the variation of the proper time distribution of the combinatorial background, has been considered: the parameters used to define the background shape, in the lifetime fit, have been varied according to their fitted errors.

The inclusion of systematic uncertainties lowers the sensitivity to 8.1 ps^{-1} without affecting the 95% C.L limit. In Table 12 the amplitude values are reported, together with their statistical and systematical errors, for five different values of $\Delta m_{B_s^0}$.

The exclusion probability of $\Delta m_{B_s^0} = 7.4\ ps^{-1}$ is 54% while the probability of obtaining a limit on $\Delta m_{B_s^0}$ higher than the actual one is 38% (Figure 15-c).
Figure 15-a and Figure 15-b represent, respectively, the error on the amplitude and the exclusion probability as a function of $\Delta m_{B_s^0}$.

$\Delta m_{B_s^0}(ps^{-1})$	A	$\sigma_A(stat)$	σ_A(total *syst.* (but t resolution))	$\sigma_A(t$ resolution *syst.*)
2.5	-0.638	0.304	0.112	0.033
5	0.037	0.400	0.118	0.060
7.5	0.182	0.561	0.069	0.098
10	1.343	0.846	0.160	0.180
12.5	0.867	1.241	0.285	0.389

Table 12: *Amplitude values with statistical and systematic errors for three different values of* $\Delta m_{B_s^0}$

7 Conclusion

A sample of 436 $D_s^{\pm}\ell^{\mp}$ candidate events has been selected from about 3.6 million hadronic Z^0 decays accumulated by DELPHI between 1992 and 1995, using seven different D_s decay modes. The number of events coming from B_s^0 semileptonic decays has been estimated to be 230 ± 18 in this sample. In addition, a sample of 441 $\phi\ell h$, containing 41 ± 12 B_s^0 semileptonic decays, has been also used. Events contained in the $D_s\ell$ sample, with a reconstructed ϕ and have been removed from this last sample.
Using these samples, three analyses have been performed. The B_s^0 lifetime has been measured and a limit on the fractional width difference between the two physical B_s^0 states has been set:

$$\tau(B_s^0) = (1.42^{+0.14}_{-0.13}(\text{stat.}) \pm 0.03(\text{syst.}))\ \text{ps}$$

$$\Delta,_{B_s^0}/,_{B_s^0} < 0.46 \text{ at the } 95\% \text{ C.L.}$$

This last result has been obtained under the hypothesis that $\tau_{B_s^0} = \tau_{B_d}$.
The study of $B_s^0 - \overline{B_s^0}$ oscillations sets a limit at 95% C.L. on the mass difference between the physical B_s^0 states:

$$\Delta m_{B_s^0} > 7.4\ \text{ps}^{-1} \text{ at } 95\% \text{ C.L.} \qquad (21)$$

with a corresponding sensitivity equal to $8.1\ \text{ps}^{-1}$.
Previous DELPHI results obtained with $D_s\ell$ and $\phi\ell$ samples ([26],[20]) are superseded by the analyses presented in this paper.

Acknowledgements

We are greatly indebted to our technical collaborators, to the members of the CERN-SL Division for the excellent performance of the LEP collider, and to the funding agencies for their support in building and operating the DELPHI detector.
We acknowledge in particular the support of
Austrian Federal Ministry of Science and Traffics, GZ 616.364/2-III/2a/98,
FNRS–FWO, Belgium,
FINEP, CNPq, CAPES, FUJB and FAPERJ, Brazil,
Czech Ministry of Industry and Trade, GA CR 202/96/0450 and GA AVCR A1010521,
Danish Natural Research Council,
Commission of the European Communities (DG XII),
Direction des Sciences de la Matière, CEA, France,

Bundesministerium für Bildung, Wissenschaft, Forschung und Technologie, Germany,
General Secretariat for Research and Technology, Greece,
National Science Foundation (NWO) and Foundation for Research on Matter (FOM), The Netherlands,
Norwegian Research Council,
State Committee for Scientific Research, Poland, 2P03B06015, 2P03B1116 and SPUB/P03/178/98,
JNICT–Junta Nacional de Investigação Científica e Tecnológica, Portugal,
Vedecka grantova agentura MS SR, Slovakia, Nr. 95/5195/134,
Ministry of Science and Technology of the Republic of Slovenia,
CICYT, Spain, AEN96–1661 and AEN96-1681,
The Swedish Natural Science Research Council,
Particle Physics and Astronomy Research Council, UK,
Department of Energy, USA, DE–FG02–94ER40817.

References

[1] M. Beneke, G. Buchalla and I. Dunietz *Phys. Rev.* **D54** (1996) 4419.

[2] L. Wolfenstein, *Phys. Rev. Lett.* **51** (1983) 1945.

[3] G. Altarelli and P.J. Franzini, *Zeit. Phys.* **C37** (1988) 271.
P.J. Franzini, *Phys Rep.* **173** (1989) 1.

[4] A. J. Buras, *Acta. Phys. Polon.* **B26** (1995) 755.

[5] A.X. El-Khadra, A. Kronfeld, P.B. Mackenzie, S.M. Ryan and J.N. Simone, *Phys. Rev.* **D58** (1998) 014506.
C. Bernard et al. (MILC Collaboration), *Phys. Rev. Lett.* **81** (1998) 4812.
D. Becirevic, Ph. Boucaud, J.P. Leroy, V. Lubicz, G. Martinelli, F. Mescia and F. Rapuano, Phys. Rev. **D60** (1999) 074501 .

[6] P. Paganini, F. Parodi, P. Roudeau and A. Stocchi, *Physica Scripta* **Vol. 58** (1998) 558.
F. Parodi, P. Roudeau and A. Stocchi, *Il Nuovo Cimento* **A112** (1999) 834.

[7] M. Beneke, G. Buchalla, C. Greub, A. Lenz and U. Nierste *Phys. Lett.* **B459** (1998) 631.

[8] ALEPH Collaboration, D. Buskulic et al., *Phys. Lett.* **B377** (1996) 205.

[9] CDF Collaboration, F. Abe et al., *Phys. Rev.* **D59** (1999) 032004.

[10] OPAL Collaboration, K. Ackerstaff et al., *Phys. Lett.* **B426** (1998) 161.

[11] DELPHI Collaboration, P. Abreu et al., Nucl. Instr. and Meth. **A378** (1996) 57.

[12] V. Chabaud et al., *Nucl. Instr. Meth.* **A368** (1996) 314.

[13] DELPHI Collaboration, P. Abreu et al., *Nucl. Phys.* **B418** (1994) 403.

[14] E.G. Anassontzis et al., *Nucl. Instr. Meth.* **A323** (1992) 351.

[15] T. Sjöstrand, *Comp. Phys. Comm.* **82** (1994) 74.

[16] DELPHI Collaboration,P. Abreu et al., *Zeit. Phys.* **C70** (1996) 531.

[17] DELPHI Collaboration, P. Abreu et al, *Zeit. Phys.* **C73** (1996) 11.

[18] N. Isgur, D. Scora, B. Grinstein and M. Wise, *Phys. Rev.* **D39** (1989) 799.

[19] Particle Data Group, *Eur. Phys. J.* **C3** (1998) 1.

[20] DELPHI Collaboration, P. Abreu et al., *Zeit. Phys.* **C71** (1996) 11.

[21] CLEO Collaboration, "D_s-Lepton Charge Correlations in B Meson Decays: A Study of the D_s Meson Production Mechanism", EPS0169 contribution to the ICHEP95, (Brussels, July 1995).

[22] E. Golowich, A. Le Yaouanc, L. Oliver, O. Pène and J.C. Raynal, *Zeit. Phys.* **C48** (1990) 89.

[23] The LEP Oscillations Working Group "LEP Combined Results on B^0 Oscillations: Results for Summer 1998 Conferences" LEPBOSC NOTE 98/3

[24] DELPHI Collaboration, W. Adam et al., *Zeit. Phys.* **C76** (1997) 579.

[25] H.G. Moser and A. Roussarie, *Nucl. Instr. and Meth.* **A384** (1997) 491.

[26] DELPHI Collaboration, W. Adam et al., *Phys. Lett.* **B414** (1997) 382.

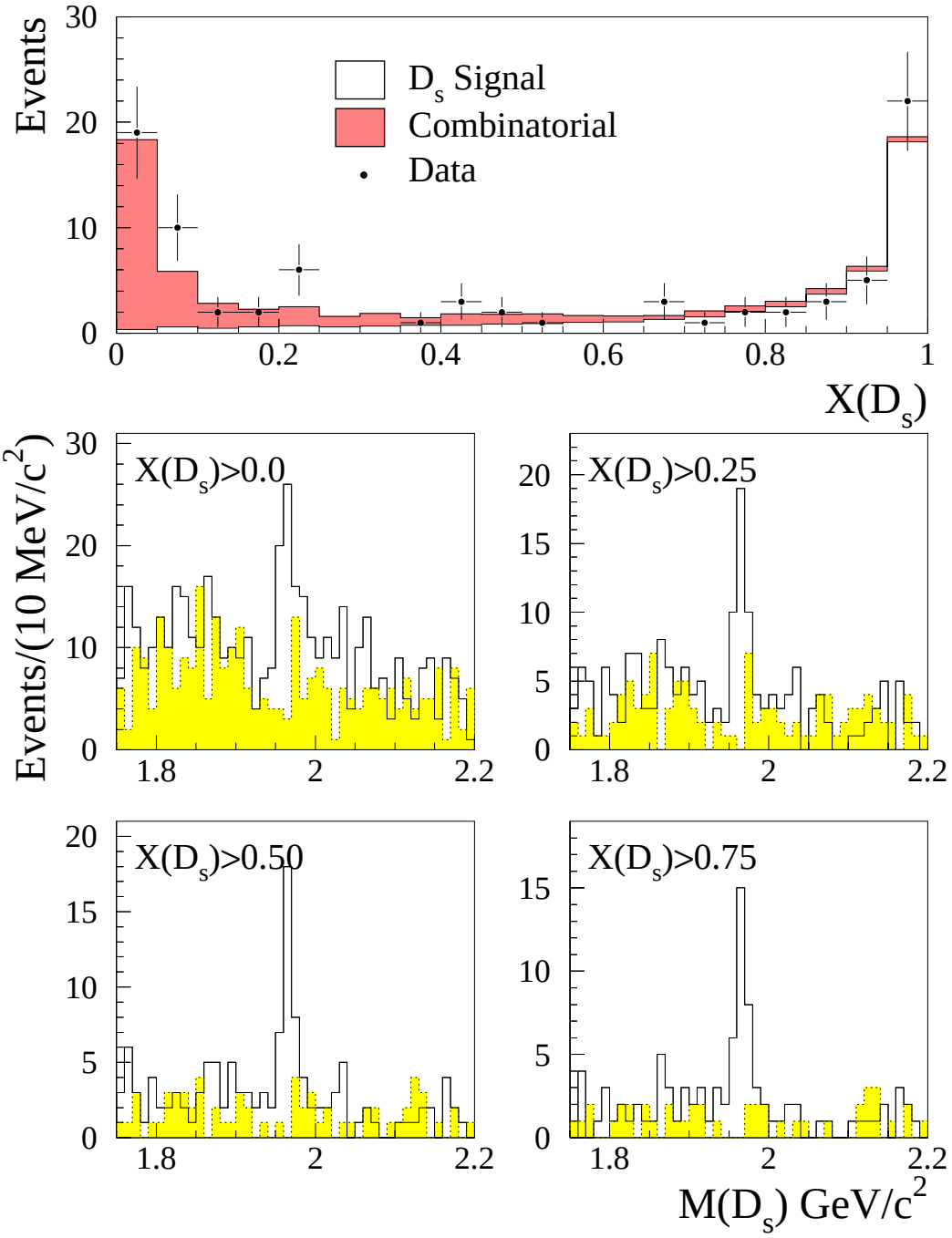

Figure 1: *The plot on the top shows the distribution of the $X_{\mathrm{D_s}}$ discriminant variable for the $\phi\pi$ channel in 94-95 data. The points with error bars represent the data, the white histogram shows the contribution from the simulated signal and the shaded histogram shows the contribution coming from simulated background events.*
It could be seen that the $X_{\mathrm{D_s}}$ is able to discriminate the signal ($\mathrm{D_s}$) from the combinatorial background.
The four figures on the bottom show the effect, on the $\phi\pi$ signal in the 94-95 data, of a cut on the discriminant variable (white histograms represent "right-sign" events while shaded histogram show "wrong-sign" events).

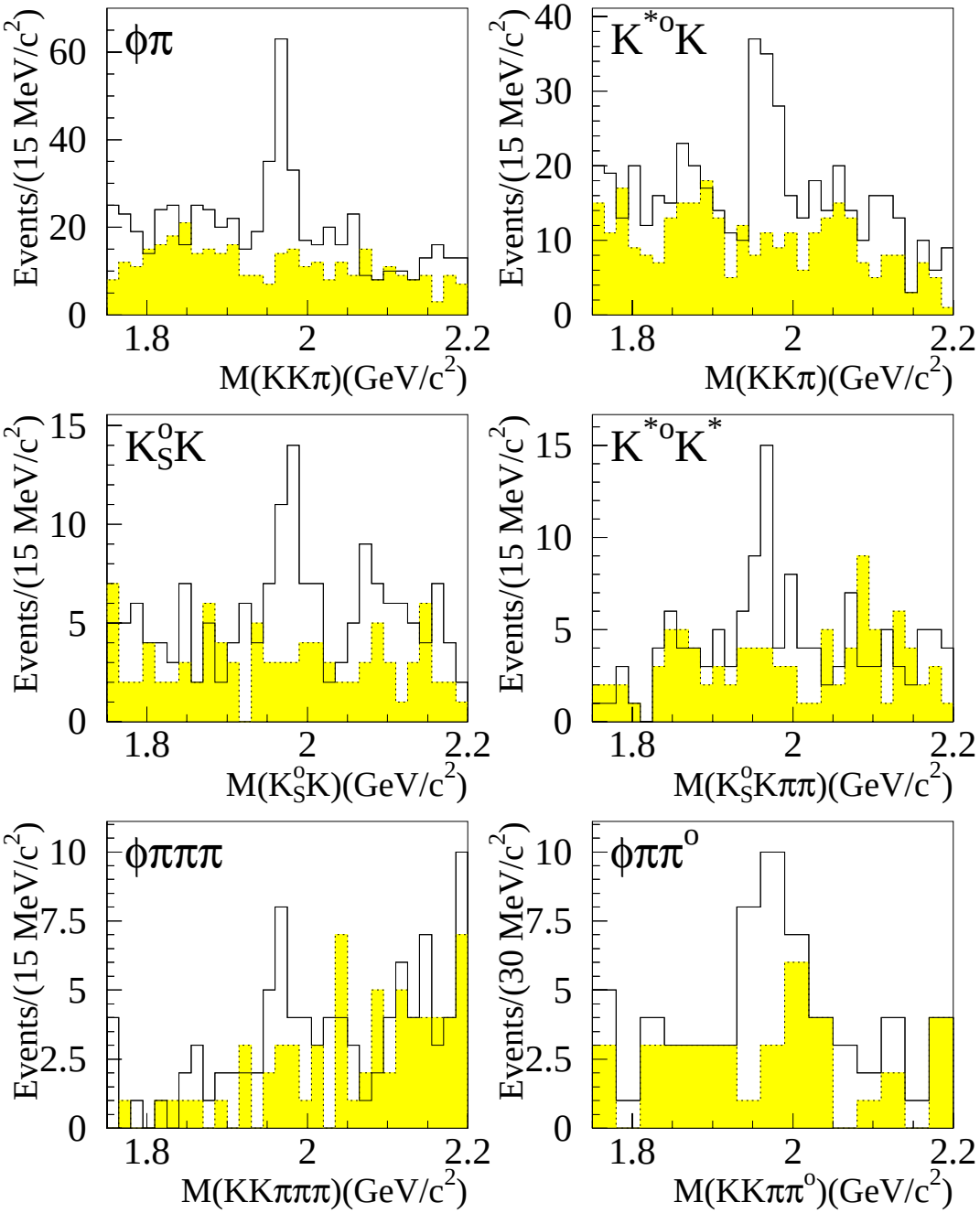

Figure 2: *Invariant mass distributions for* D_s *candidates in six non-leptonic decay modes* ($\phi\pi^+$, $\overline{K}^{*0}K^+$, K^0K^+, $\overline{K}^{*0}K^{*+}$, $\phi\pi^+\pi^-\pi^+$ *and* $\phi\pi^+\pi^0$). *The last three decay modes have been reconstructed using only the 94-95 statistics. The corresponding distribution for wrong-sign combinations are given by the shaded histograms*

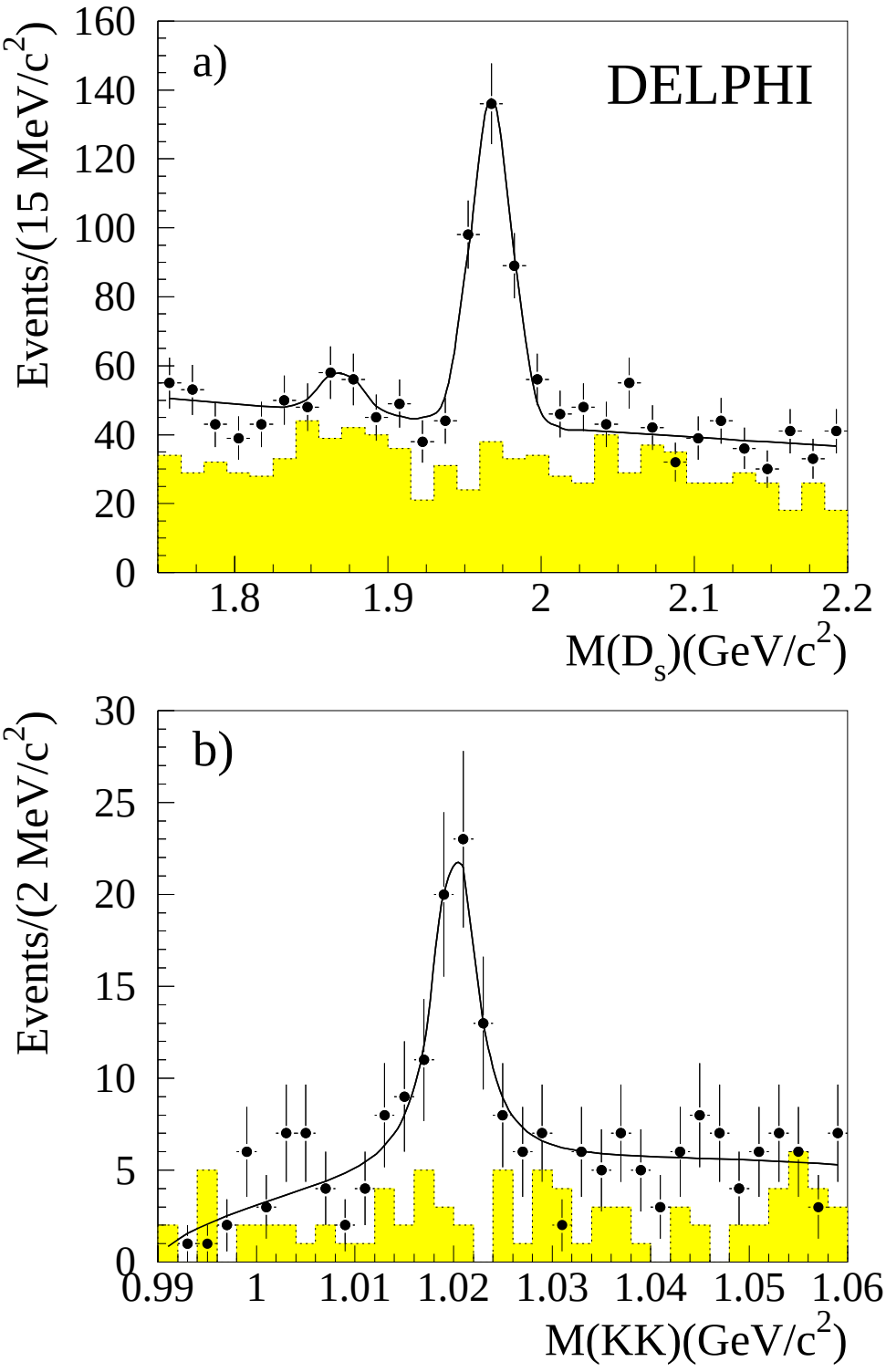

Figure 3: *a) Invariant mass distributions for* $\mathrm{D_s}$ *candidates in non-leptonic decay modes* ($\phi\pi^+$, $\overline{\mathrm{K}}^{*0}\mathrm{K}^+$, $\mathrm{K}^0\mathrm{K}^+$, $\overline{\mathrm{K}}^{*0}\mathrm{K}^{*+}$, $\phi\pi^+\pi^-\pi^+$ *and* $\phi\pi^+\pi^0$). *b)* $\mathrm{K}^+\mathrm{K}^-$ *invariant mass distribution for* $\mathrm{D_s}$ *candidates selected in the two semileptonic decay modes. The corresponding distribution for wrong-sign combinations are given by the shaded histograms. The curves show the result of fits described in the text.*

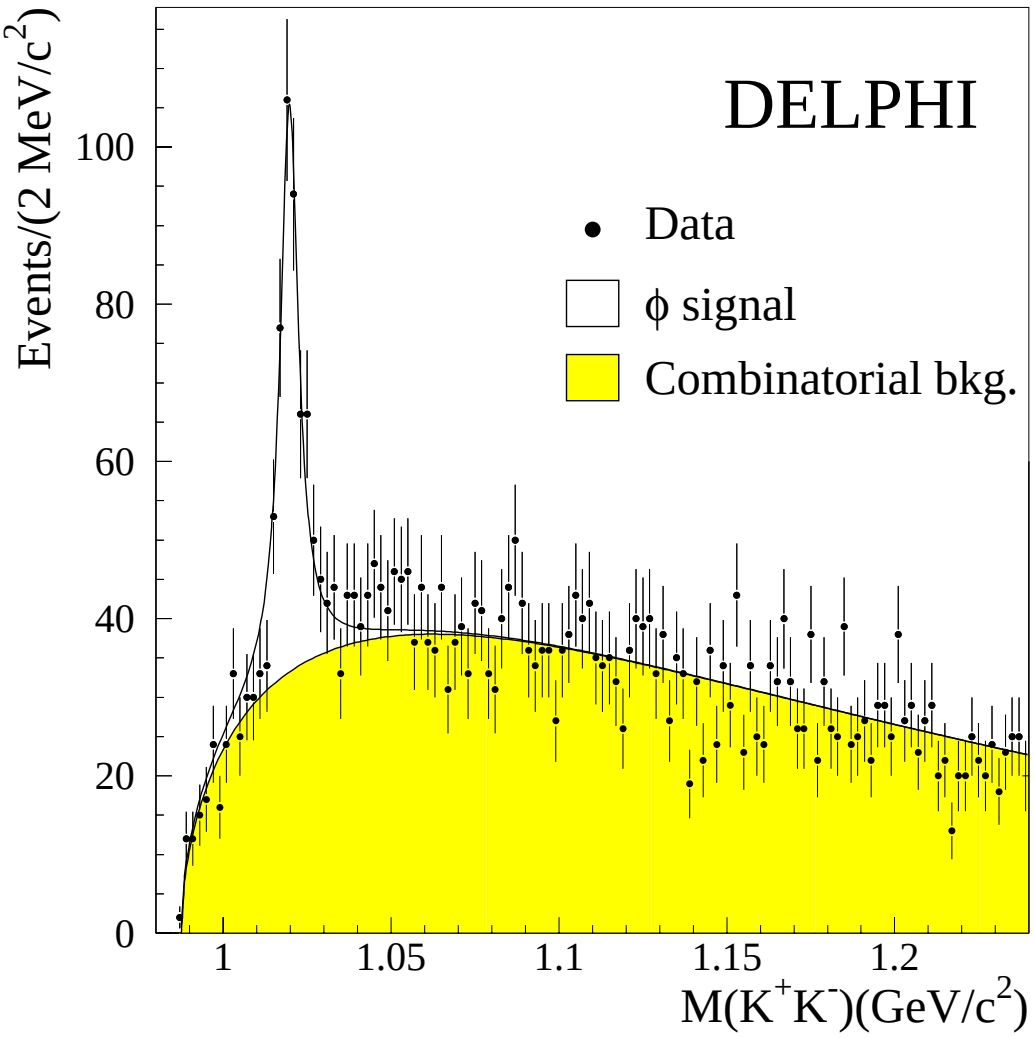

Figure 4: *K^+K^- invariant mass distribution of the $\phi\ell h$ candidates. The curves show the result of the fit described in the text (the signal and the combinatorial background components are represented by the white and shaded histograms respectively).*

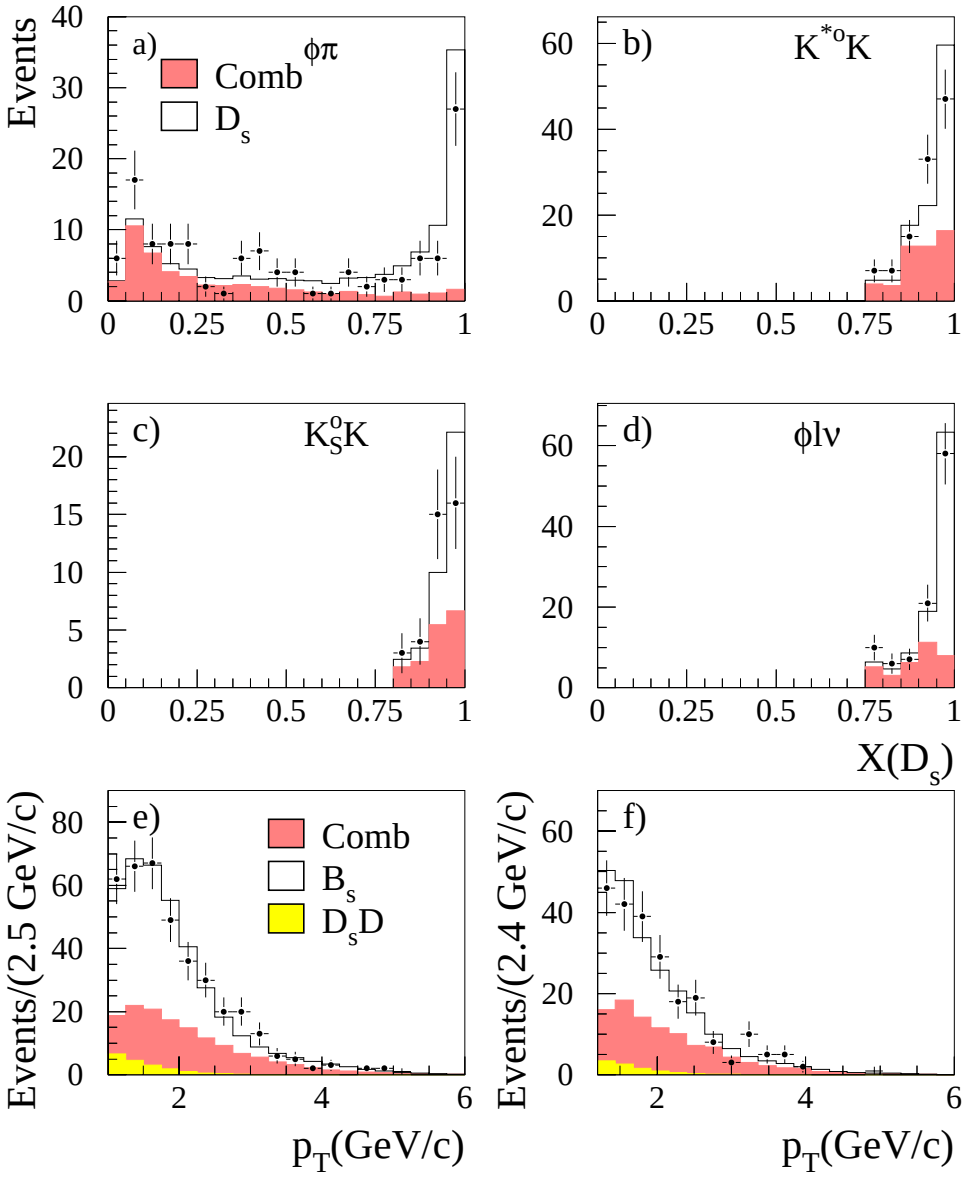

Figure 5: *The plots illustrate the agreement between data and simulation for the variables used in the estimate of the* B_s^0 *purity on an event by event basis.*
a),b),c) and d) show the X_{D_s} *distributions for the channels* $\phi\pi$, $\overline{K^{0*}}K$, K_S^0K *and* $\phi\ell^+$ *respectively. White histograms and shaded histograms represent the signal and the background respectively.*
e) and f) show the p_T *distributions for the samples selected with* $p_T > 1$ *GeV/c* ($\phi\pi^+$ *and* $\phi\ell^+\nu$) *and* $p_T > 1.2$ *GeV/c (all the others) respectively.*
For the p_T *distribution the* $D_s\overline{D}$ *and the combinatorial background are considered separately.*

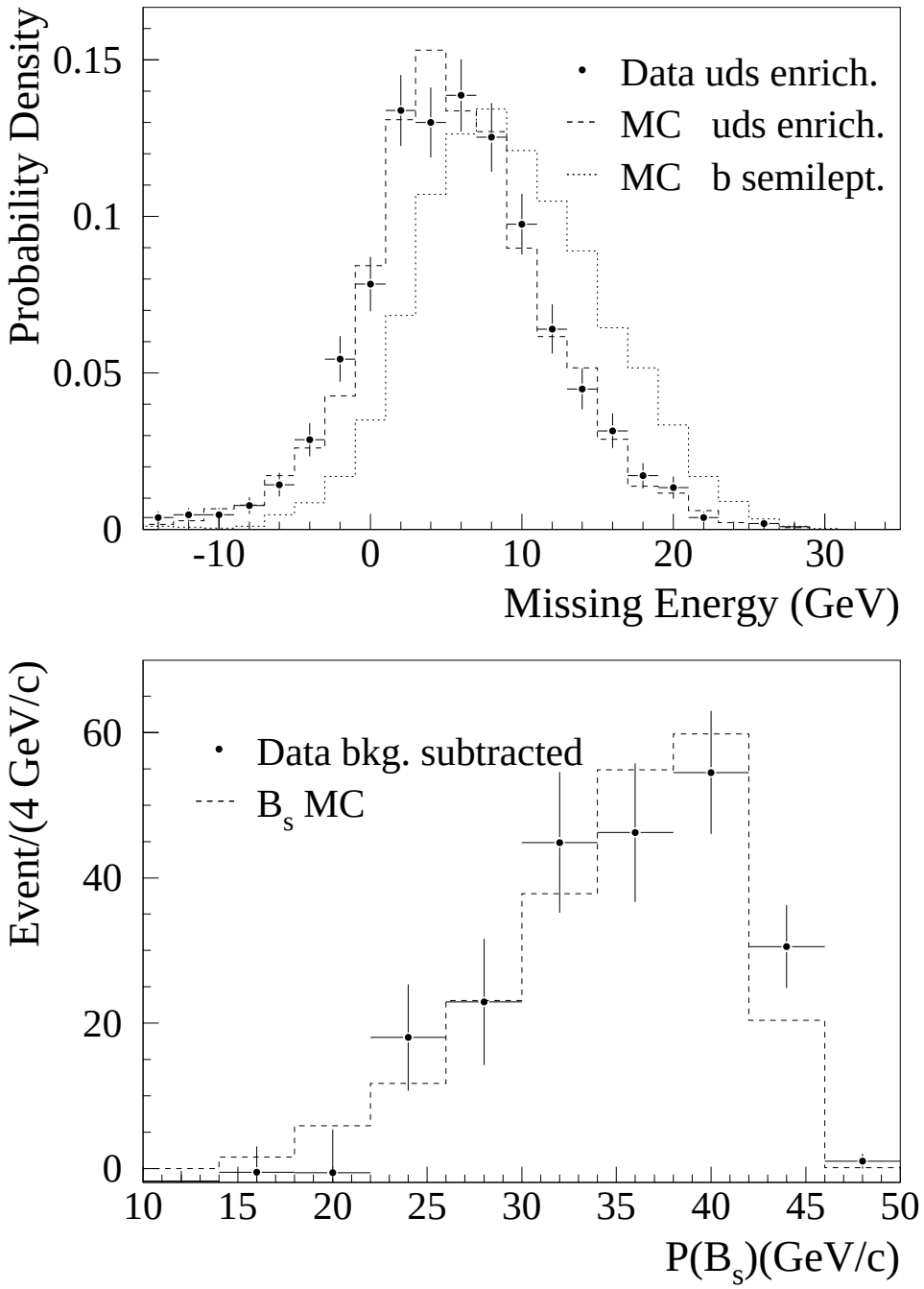

Figure 6: *The plot on the top shows the comparison between data and the simulation for the missing energy distribution after correction (see Section 3.6). The data (dots with error bars) and the simulation (dashed histogram) are enriched in light quark events. The dotted histogram shows the missing energy distribution in simulated b semileptonic decays. The plot on the bottom shows the comparison between the* B_s^0 *momentum distribution for simulated events and the one estimated from data in the signal region by subtracting the* B_s^0 *momentum distribution of events in the* D_s *side bands from that of the events in the signal region.*

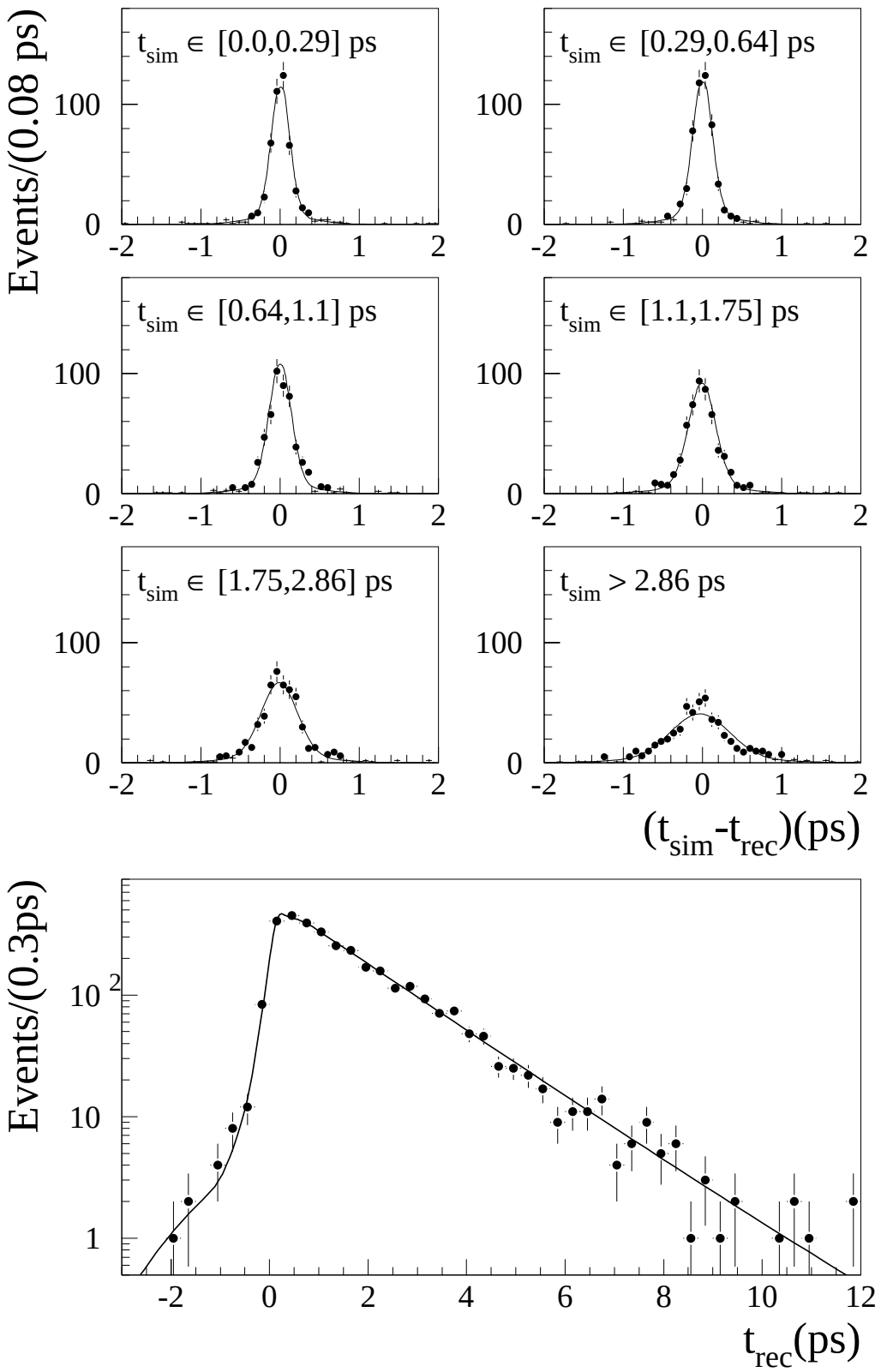

Figure 7: *The six plots on the top show the proper time resolution, defined as the difference between the generated time (t_{sim}) and the reconstructed time (t_{rec}), in bins of generated time on a sample of $\phi\pi$ events simulated with the 94-95 Vertex Detector configuration. The plot on the bottom shows the distribution of the reconstructed time with the fit superimposed.*

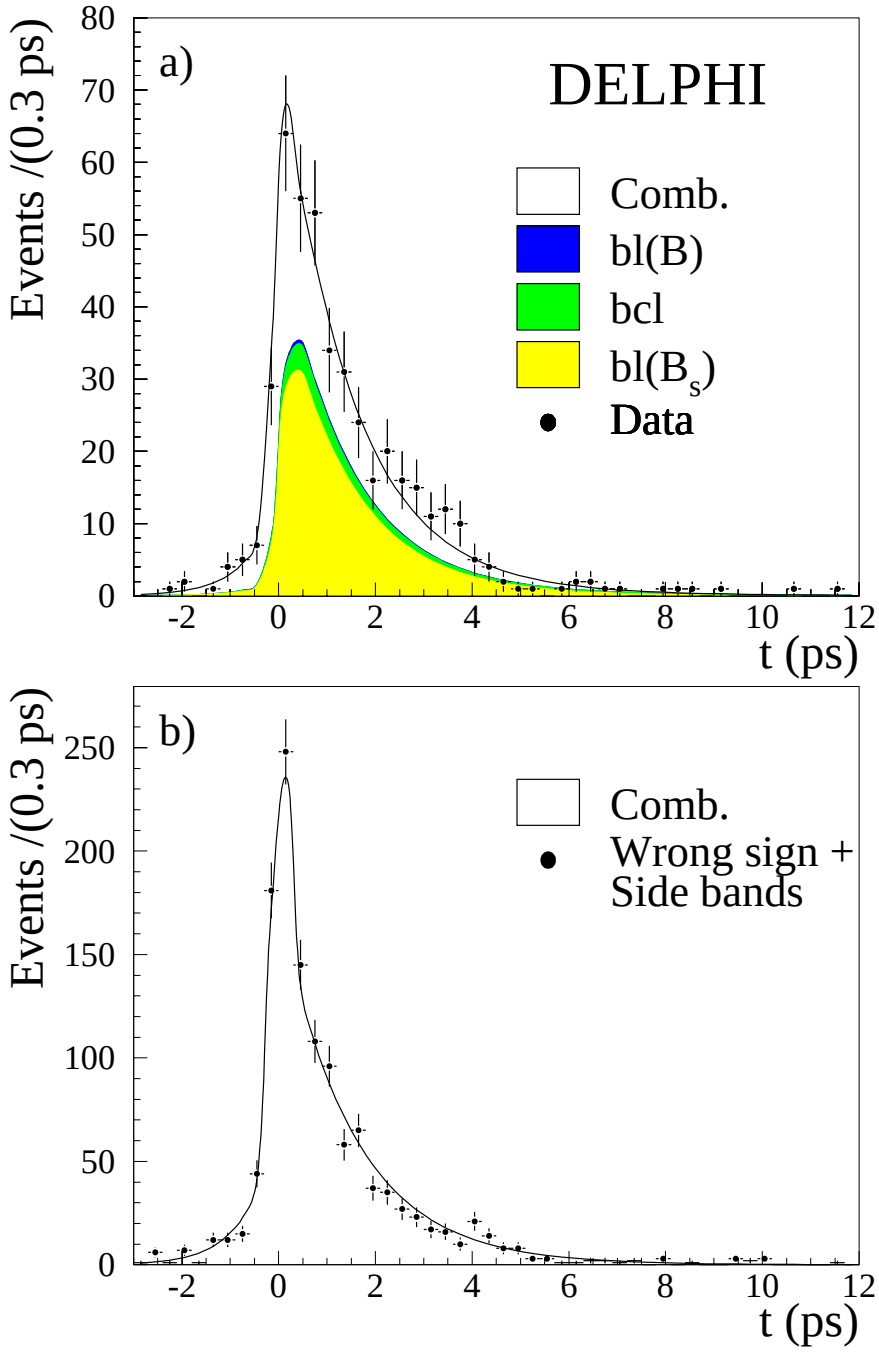

Figure 8: $D_s\ell$ *sample. a) Likelihood fit for events in the signal mass region. The points show the data and the curves correspond to the different contributions to the selected events. b) The same as a) but for "wrong-sign" events and for events situated in the side band region.*
The labels of the signal components refers to Section 3.5.1

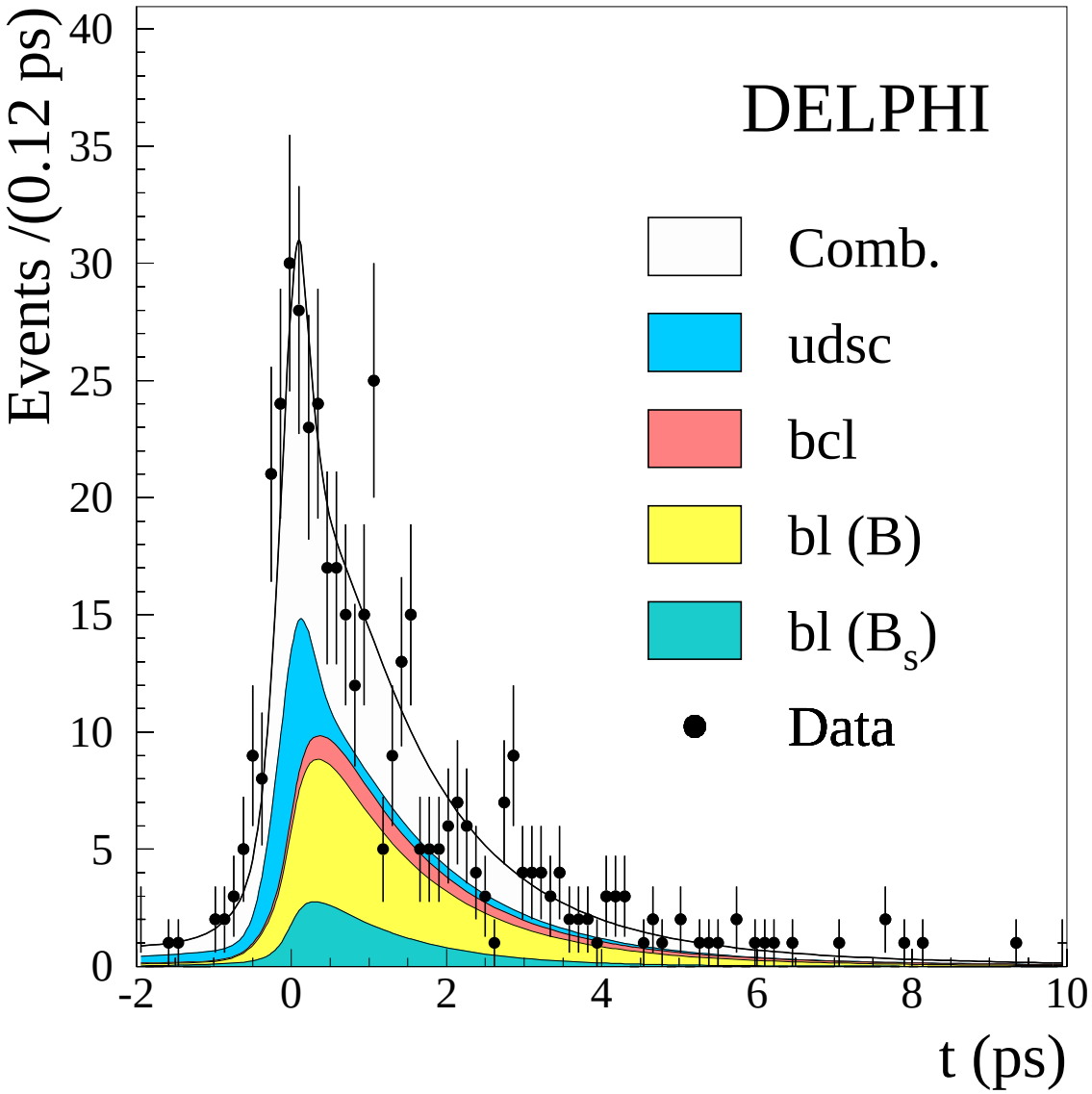

Figure 9: *$\phi\ell h$ sample.*
Likelihood fit for events in the signal mass region. The points show the data and the curves correspond to the different contributions to the selected events.
The labels of the signal components refers to Section 3.5.2

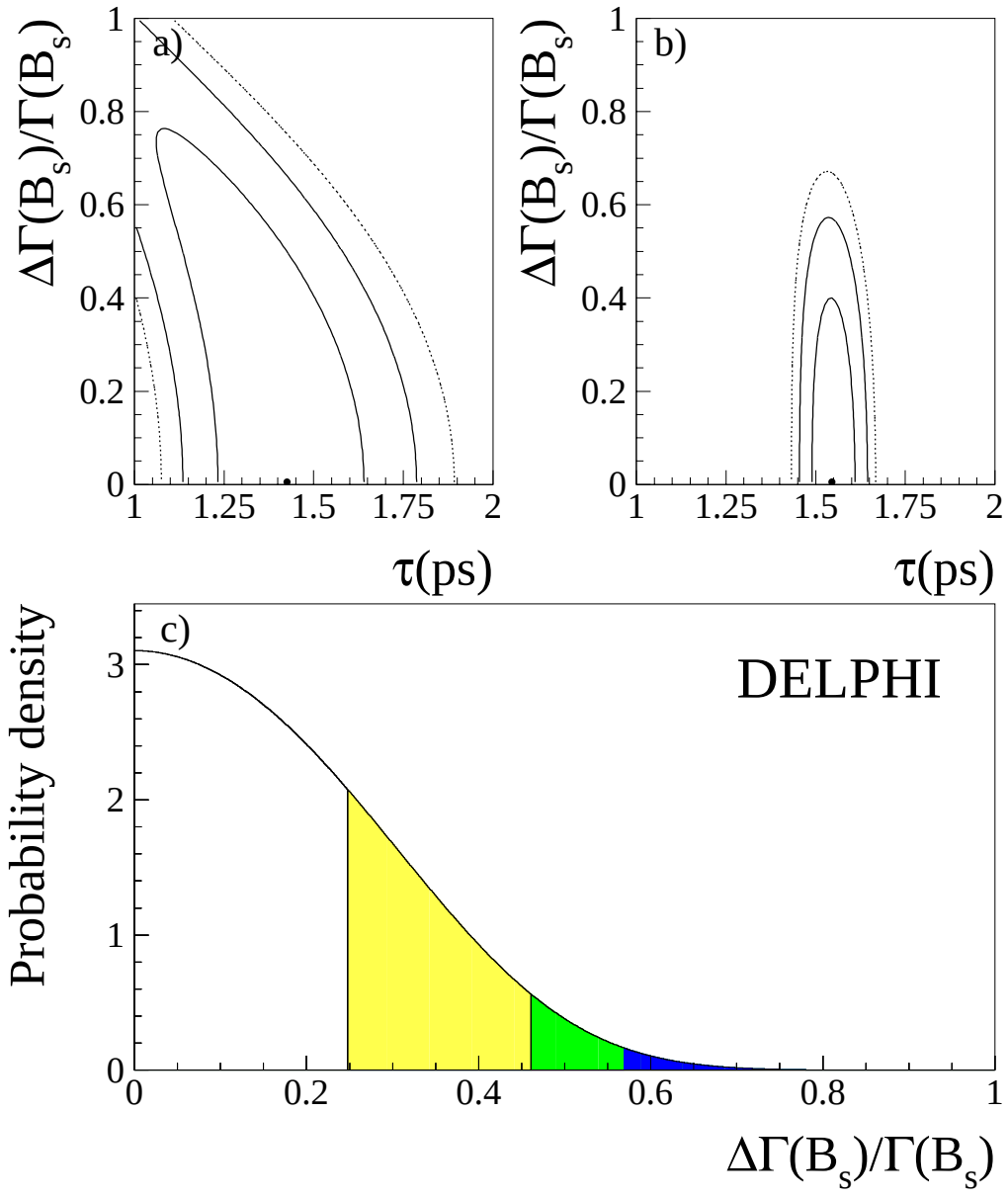

Figure 10: *a) 68%, 95% and 99% C.L. contours of the negative log-likelihood in the plane* $\tau(\equiv 1/$, $_{B_s}$)-Δ, $_{B_s^0}/$, $_{B_s^0}$ *evaluated on the* $D_s\ell$ *sample. b) Same as a) but with the constraint* $\tau = \tau_{B_d^0}$. *c) Probability density distribution for* Δ, $_{B_s^0}/$, $_{B_s^0}$*; the three shaded regions show the limits at 68 %, 95% and 99% C.L. respectively.*

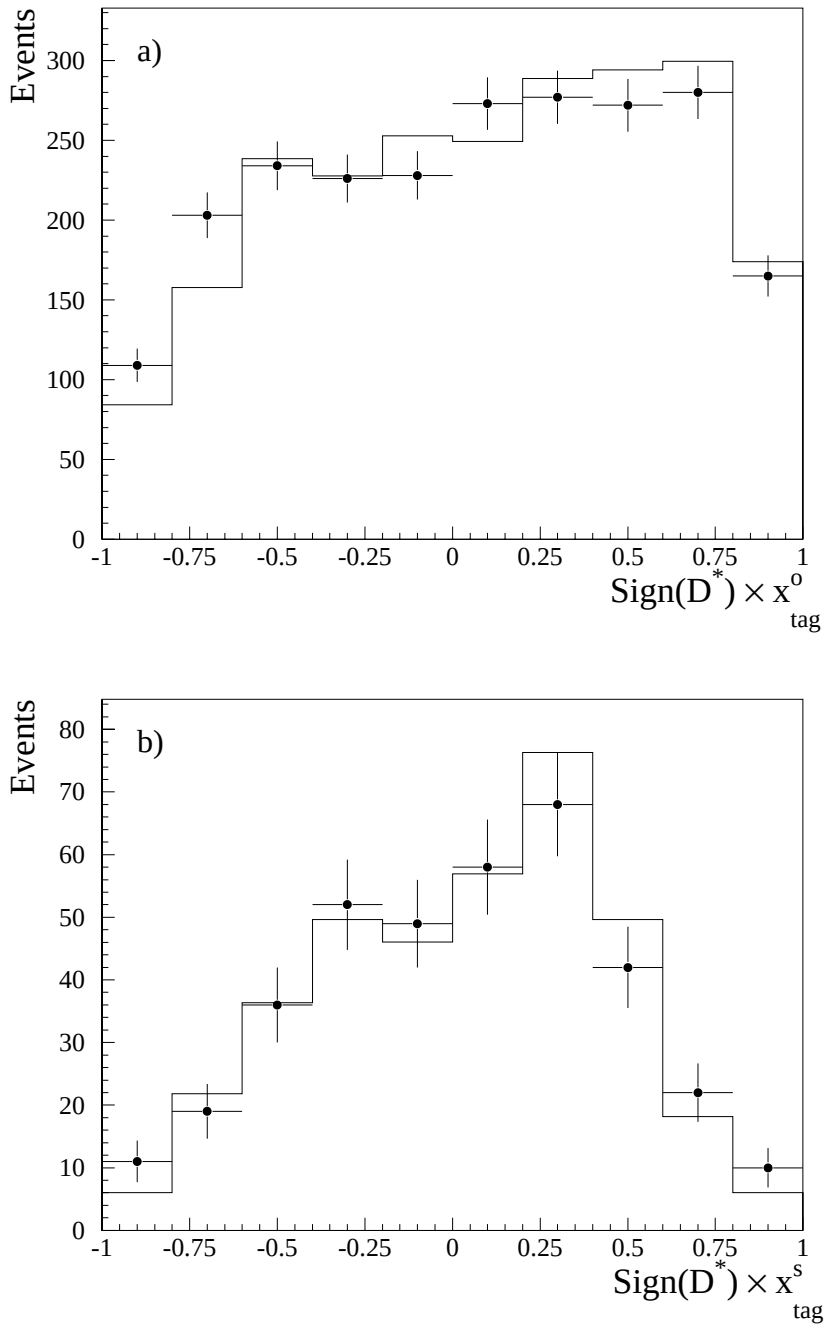

Figure 11: *Check of the flavour tagging on the* D^* *sample.*
a) Distribution of the product between the global tagging variable x^o_{tag} *and the charge of the* $D^{*\pm}$ *in the hemisphere opposite to the* $D^{*\pm}$ *candidate.*
b) Distribution of the product between the global tagging variable x^s_{tag} *and the charge of the* $D^{*\pm}$ *in the same hemisphere as the* $D^{*\pm}$*-lepton candidate.*
The full dots with the error bars represent the data. The histogram is obtained in the simulation.
The non perfect separation is due to the mistag fraction of x_{tag} *but also to the* $\mathrm{B^0_d}$-$\overline{\mathrm{B^0_d}}$ *mixing.*

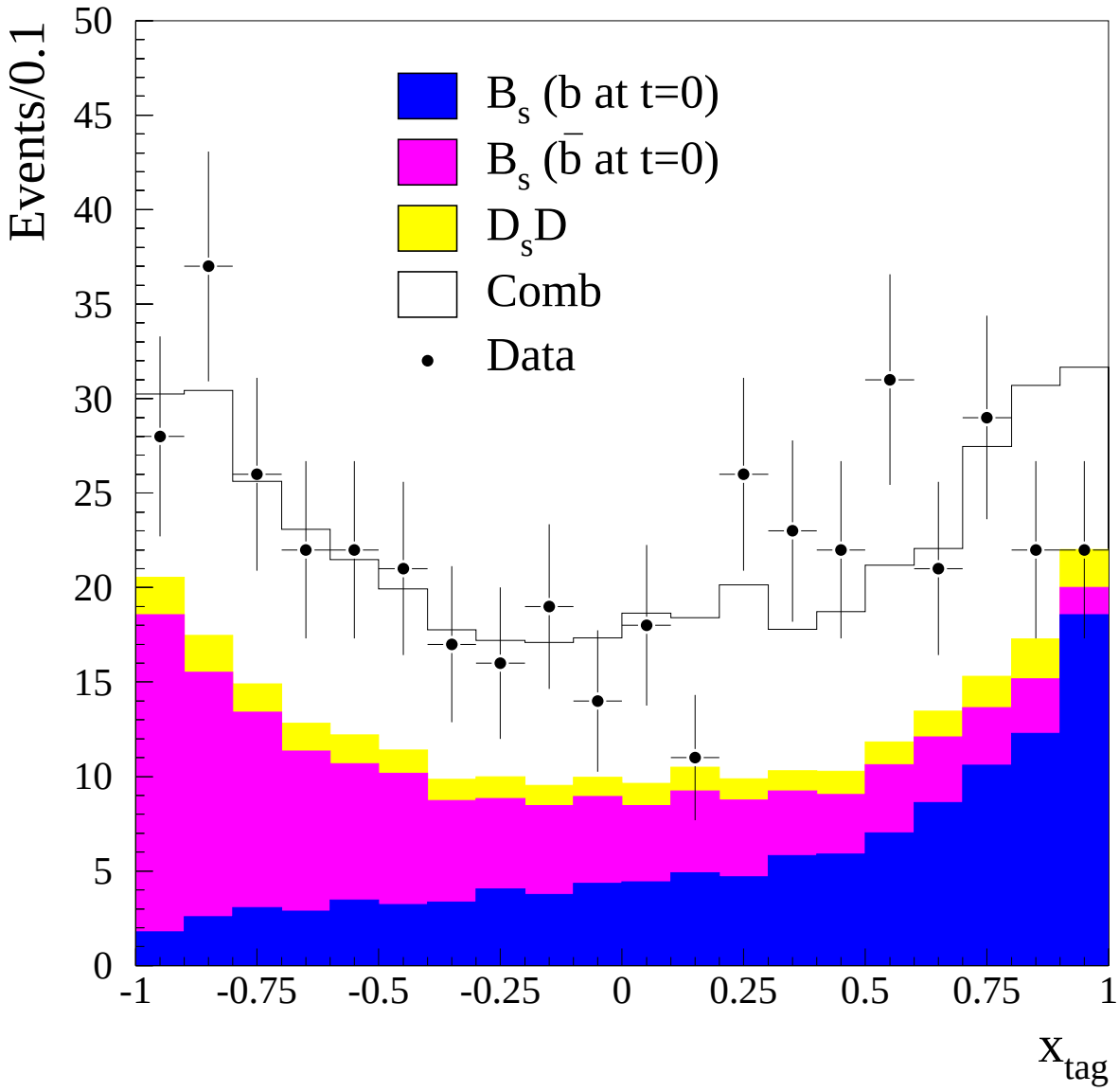

Figure 12: *The plot shows the distribution of the x_{tag} discriminant variable in the $D_s\ell$ sample. The points with the error bars represent the data, the white histogram shows the contribution from combinatorial background, the lighter histogram the contribution from D_sD events and the darker histograms the contribution from the B_s^0 signal in which B_s^0 mesons produced from b or $\bar{b}$ quarks have been distinguished.*
The degree of separation between the b and $\bar{b}$ histograms quantify the tagging purity of x_{tag}.

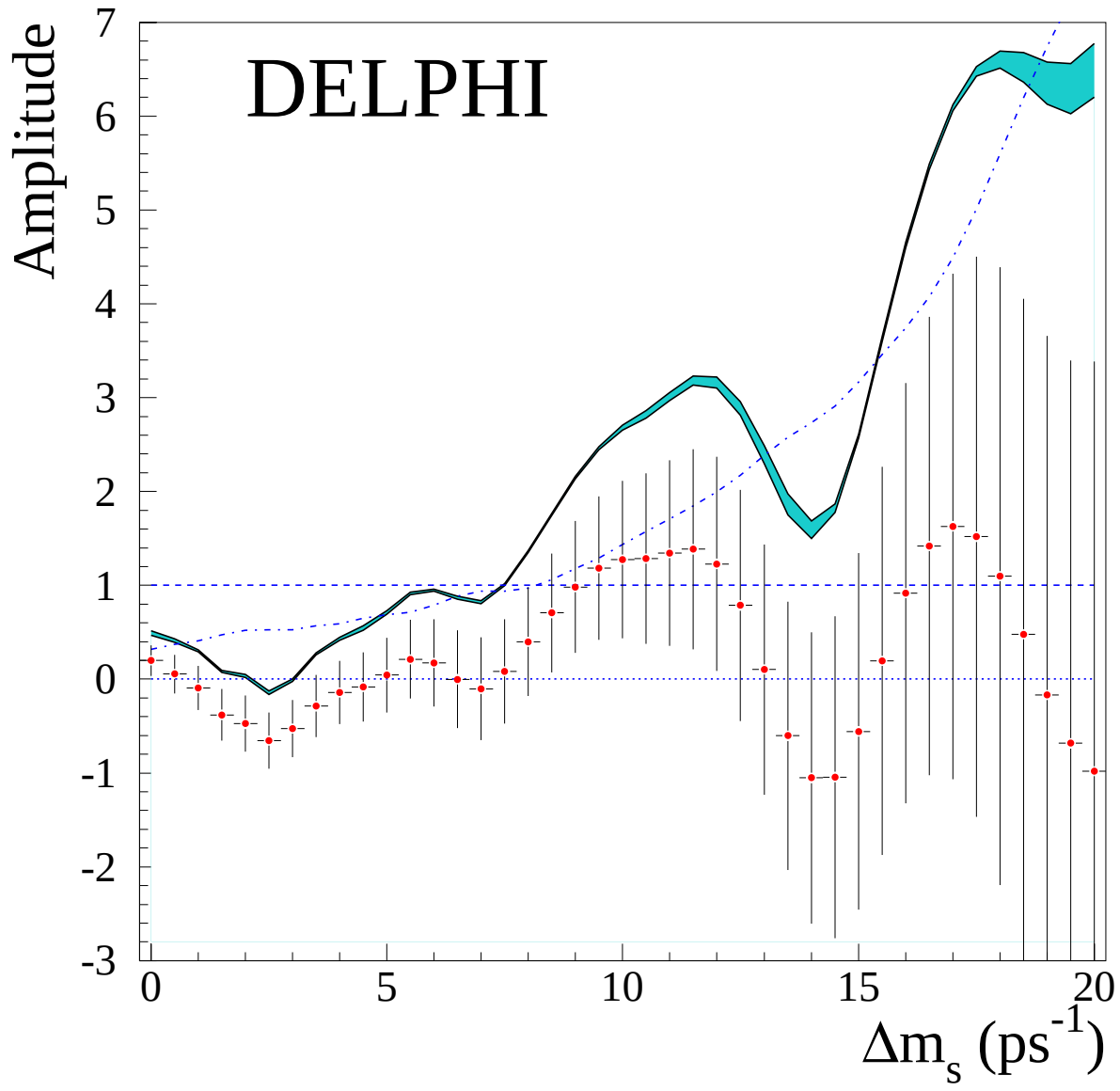

Figure 13: *Variation of the oscillation amplitude A as a function of Δm_s. The lower continuous line corresponds to $A + 1.645\ \sigma_A$ where σ_A includes statistical uncertainties only, while the shaded area includes the contribution from systematics. The dashed-dotted line corresponds to the sensitivity curve. The lines at A=0 and A=1 are also given.*

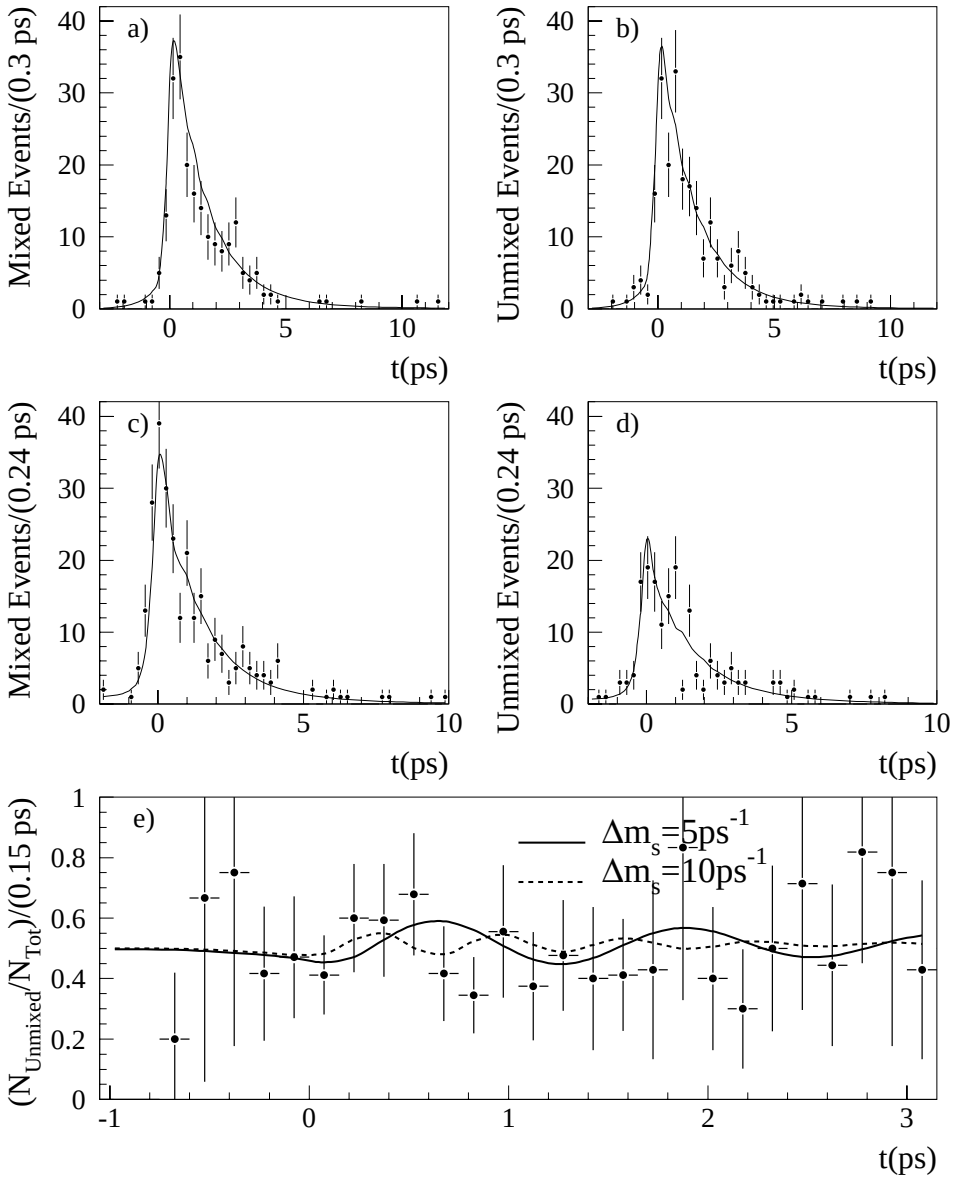

Figure 14: *Proper time distribution of mixed and unmixed events in* $\mathrm{D_s}\ell$ *sample (a-b) and in the* $\phi\ell$ *sample (c-d); the full dots with error bars represent the data, the curves are the corresponding distributions for* $\Delta m_{\mathrm{B_s^0}} = 10\ ps^{-1}$.
c) Ratio between the mixed events and the total number of events in bins of proper time in the $\mathrm{D_s}\ell$ *sample. The full (dashed) line represents the prediction for an oscillation* ($A = 1$) *with* $\Delta m_{\mathrm{B_s^0}} = 5\ ps^{-1} (10\ ps^{-1})$.

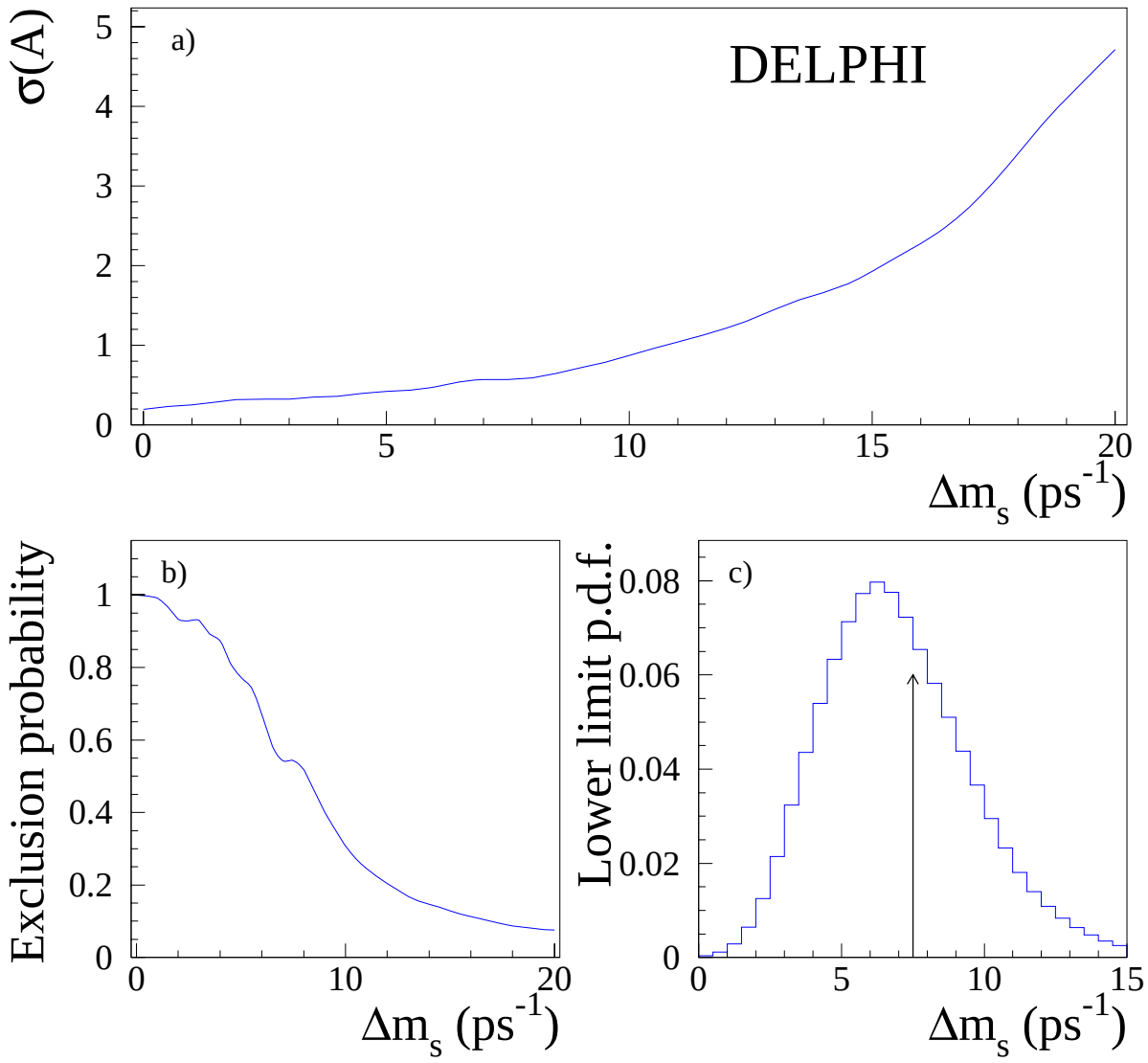

Figure 15: *a) Variation of the error on the amplitude as a function of Δm_s. b) Exclusion probability vs. Δm_s. c) Lower limit probability density function vs. Δm_s.*